Cell Reports

Article

Leishmania parasites exchange drug-resistance genes through extracellular vesicles

Graphical abstract

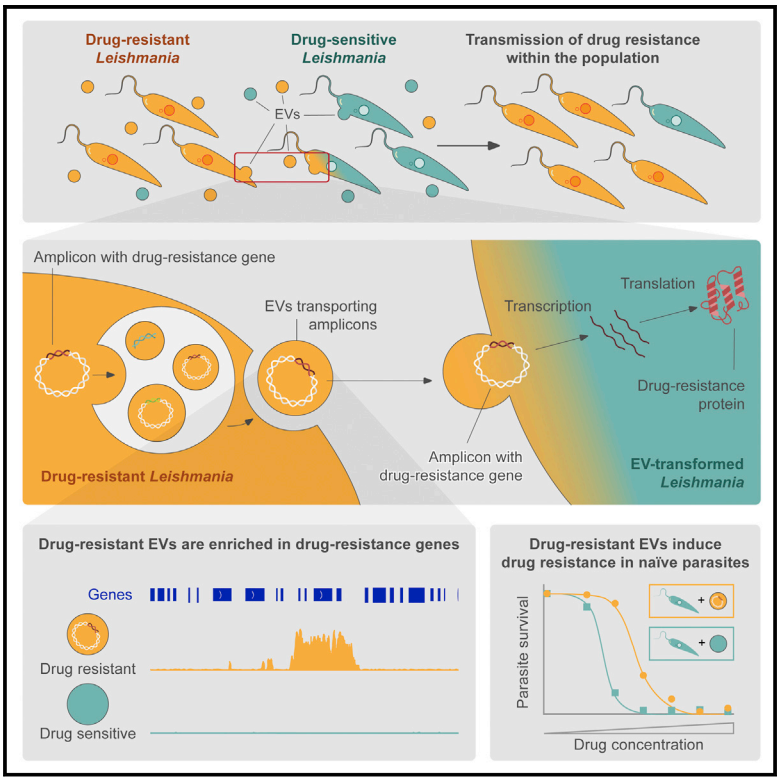

Authors

Noélie Douanne, George Dong, Atia Amin, ..., David Langlais, Martin Olivier, Christopher Fernandez-Prada

Correspondence

martin.olivier@mcgill.ca (M.O.), christopher.fernandez.prada@umontreal.ca (C.F.-P.)

In brief

Douanne et al. demonstrate that extracellular vesicles (EVs) released by drug-resistant *Leishmania* are enriched in genomic regions containing drug-resistance genes. Moreover, circular amplicons containing drug-resistance genes can exploit EVs to guarantee efficient propagation into naive, sensitive parasites, leading to the emergence of drug-resistant subpopulations.

Highlights

- EVs serve as a mechanism of genetic exchange in *Leishmania* parasites
- DNA content of EVs reflects the genetic background of the source parasite
- Drug-resistant *Leishmania* transfer resistance genes through EVs
- EVs from resistant parasites improve the growth and fitness of naive parasites

Douanne et al., 2022, Cell Reports *40*, 111121
July 19, 2022
https://doi.org/10.1016/j.celrep.2022.111121

CellPress

Cell Reports

CellPress
OPEN ACCESS

Article

Leishmania parasites exchange drug-resistance genes through extracellular vesicles

Noélie Douanne,[1,2] George Dong,[3,7] Atia Amin,[4,7] Lorena Bernardo,[1,2] Mathieu Blanchette,[5] David Langlais,[4,6] Martin Olivier,[3,6,*] and Christopher Fernandez-Prada[1,2,6,8,*]

[1]Department of Pathology and Microbiology, Faculty of Veterinary Medicine, Université de Montréal, 626 CIMIA Sicotte Street, Saint-Hyacinthe, QC J2S 2M2, Canada
[2]The Research Group on Infectious Diseases in Production Animals (GREMIP), Faculty of Veterinary Medicine, University of Montreal, Saint-Hyacinthe, QC J2S 2M2, Canada
[3]IDIGH, The Research Institute of the McGill University Health Centre, 2155 Guy Street, Montreal, QC H3H 2L9, Canada
[4]Department of Human Genetics, McGill University Genome Centre, Montreal, QC H3A 0G1, Canada
[5]School of Computer Science, McGill University, Montreal, QC H3A 0E9, Canada
[6]Department of Microbiology and Immunology, McGill Research Centre on Complex Traits, Montreal, QC, Canada
[7]These authors contributed equally
[8]Lead contact
*Correspondence: martin.olivier@mcgill.ca (M.O.), christopher.fernandez.prada@umontreal.ca (C.F.-P.)
https://doi.org/10.1016/j.celrep.2022.111121

SUMMARY

Leishmania are eukaryotic parasites that have retained the ability to produce extracellular vesicles (EVs) through evolution. To date, it has been unclear if different DNA entities could be associated with *Leishmania* EVs and whether these could constitute a mechanism of horizontal gene transfer (HGT). Herein, we investigate the DNA content of EVs derived from drug-resistant parasites, as well as the EVs' potential to act as shuttles for DNA transfer. Next-generation sequencing and PCR assays confirm the enrichment of amplicons carrying drug-resistance genes associated with EVs. Transfer assays of drug-resistant EVs highlight a significant impact on the phenotype of recipient parasites induced by the expression of the transferred DNA. Recipient parasites display an enhanced growth and better control of oxidative stress. We provide evidence that eukaryotic EVs function as efficient mediators in HGT, thereby facilitating the transmission of drug-resistance genes and increasing the fitness of cells when encountering stressful environments.

INTRODUCTION

Parasitic infectious diseases remain real and pervasive threats worldwide. The situation has worsened in recent decades due to the emergence and spread of drug resistance. In particular, the vector-borne parasite *Leishmania* affects 15 million people worldwide, and in the absence of effective preventive and therapeutic treatments, is spreading with almost 1.5 million new cases every year (Fernández-Prada et al., 2019). Control of the disease is based on a very short list of chemotherapeutic agents headed by antimonial drugs (Sb), followed by miltefosine (MF) and amphotericin B (AmB). These drugs are far from ideal due to host toxicity, limited access, and high rates of drug resistance (Fernández-Prada et al., 2019; Sundar and Singh, 2018).

One of the most striking evolutionary features of *Leishmania* is the lability of its genomic architecture, which can be conveniently restructured to rapidly counter stressors such as drug pressure (Bussotti et al., 2018; Leprohon et al., 2009; Ubeda et al., 2008). As *Leishmania* is an early divergent eukaryote, it lacks classic transcriptional control mechanisms. *Leishmania* parasites mostly rely on aneuploidy and DNA copy number variations (CNVs) for regulation of the expression of drug targets, stress-related genes, and drug-resistance genes (Leprohon et al., 2009; Ubeda et al., 2014). Increases in CNVs in drug-resistant *Leishmania* parasites are frequently caused by the reversible accumulation of small extrachromosomal amplifications (i.e., amplicons) containing drug-resistance genes. These are generated through homologous recombination events between direct repeated sequence elements (producing circular amplicons) or inverted ones (producing linear amplicons), when *Leishmania* is exposed to stressful environmental conditions (El Fadili et al., 2005; Guimond et al., 2003; Leprohon et al., 2009; Ubeda et al., 2008, 2014). Of note, the presence of extrachromosomal episomes has been repeatedly confirmed in both *in vitro*-generated drug-resistant strains and field isolates (Downing et al., 2011; Leprohon et al., 2009; Mukherjee et al., 2007; Tripp et al., 1991; Ubeda et al., 2008, 2014).

Extracellular vesicles (EVs) are nanometric membrane-enclosed particles released into the extracellular space by organisms belonging to almost all living kingdoms; they serve as mediators of intercellular communication (Dong et al., 2021; Yáñez-Mó et al., 2015). In this way, EVs have emerged as key players in *Leishmania* biology by leading to, *inter alia*, an enrichment of parasite populations with key virulence factors (i.e., GP63) during the first moments of infection, promotion of parasite survival, or the triggering of an exacerbation of the disease

(Atayde et al., 2015; da Silva Lira Filho et al., 2022; Dey et al., 2018; Hassani et al., 2014; Silverman et al., 2010). Recently, our group made the discovery that small EVs contain specific protein signatures reflecting the drug-resistance profile of the parental *Leishmania* strain from which they originate (Douanne et al., 2020a). Moreover, we showed that *Leishmania* EVs can serve as a viral envelope for the endovirus *Leishmania* RNA virus 1 (LRV1), facilitating virus transmission and increasing infectivity in the mammalian host (Atayde et al., 2019).

These two seminal findings prompted us to explore whether EVs could be involved in the acquisition of drug-resistance genes through horizontal transfer events. Herein, we provide evidence that EVs released by drug-resistant *Leishmania* parasites are enriched in genomic regions containing genes involved in drug resistance. Moreover, we show that those circular amplifications containing drug-resistance genes can exploit EVs to guarantee efficient propagation into naive, drug-sensitive parasites (both intra- and interspecies), leading to the rapid emergence of drug-resistant subpopulations. This biological mechanism, coupled with *Leishmania*'s genomic plasticity, could contribute to a rapid genomic diversification of a parasite population, while promoting rapid fitness gains in hostile environments.

RESULTS

EV DNA is highly enriched in drug-resistance genes reflecting the parental parasite

From our recent study showing that *Leishmania* EVs can serve as a cell-to-cell shuttle for double-stranded RNA viruses (Atayde et al., 2019), we hypothesized that this could also be the case for genes encoding proteins involved in drug resistance in *Leishmania*. To prove this, we selected a panel of drug-sensitive and drug-resistant strains belonging to *L. infantum* and *L. major* (Figure 1). First, the various strains were analyzed in terms of drug sensitivity to confirm their previously reported phenotypes (Table S1). Next, EVs were purified and assessed in terms of size and distribution (Figure 1A), particle-to-protein ratio (Figure 1B), and transmission electron microscopy (TEM) (Figure 1C). For all strains, vesicle purifications yielded EVs mostly situated under the 200 nm threshold (Figure 1A), therefore corresponding to small EVs. The ratio of particles per microgram of protein was above 10^{11} for all the extractions, which corresponds to highly pure EV preparations (Bellotti et al., 2021) (Figure 1B). TEM experiments revealed EV preparations to be free of contaminants and homogeneous in size (Figure 1C).

To confirm whether leishmanial EVs could serve as amplicon "carriers," we isolated and characterized the DNA associated with the EVs released by the *L. infantum* wild type (*Ldi* WT) and the *L. infantum* Sb2000.1 (*Ldi* Sb) strains, the latter known to be equipped with a circular amplicon containing the *mrpA* gene (responsible for Sb resistance). DNA was recovered from EVs of three independent cultures of *Ldi* WT and *Ldi* Sb and analyzed by DNA sequencing (DNA-seq) using short-read Illumina sequencing (Data S1). Whole-genome sequencing (WGS) was also performed to generate high-coverage comparative datasets for the EV DNA analysis. The reads were aligned on the LINF reference genome assembly and a differential abundance analysis was performed by comparing the normalized read coverage in *Ldi* Sb and *Ldi* WT for 5 kb genomic intervals, tilling each chromosome. This analysis highlights some CNVs at the genomic level (Figure 2A; outer circle), which are also reflected in the DNA recovered from EVs (inner circle). For example, as shown on the Miami plot representation of chromosome LinJ6 (Figures S1A and S1B), the terminal portion exhibits a 5-fold amplification in *Ldi* WT. In contrast, a segment of LinJ17 (between 157 and 193 kb) was depleted in the WT strain (Figures S1C and S1D). As expected, the WGS analysis detected the previously described *mrpA*-containing amplicon stemming from LinJ23, with an ~30-fold increased coverage in *Ldi* Sb parasites (Figures 2B and 2C). Importantly, the DNA isolated from EVs of Sb-resistant parasites also exhibited a similar increase in sequence coverage over this ~16 kb region (Figures 2B and 2C).

To validate our DNA-seq findings, we conducted a series of PCR experiments targeting either the 4.7 kb *mrpA* complete open reading frame (ORF) or a 1.8 kb DNA fragment resulting from a homologous recombination event during the formation of the extrachromosomal circular DNA (Figure 2D), and thus absent from the sequence of the chromosomal locus (Leprohon et al., 2009). As shown in Figure 2E, the *mrpA* gene was amplified when using both total DNA and EV DNA from the Sb2000.1 strain as a template, but only from the genomic DNA recovered from *Ldi* WT (Figure 2E). However, the amplicon junction was detectable only in DNA isolated from the Sb-resistant strain (in both total DNA and EV DNA; Figure 2E), further confirming the presence of this extrachromosomal element in drug-resistant EVs. Finally, we evaluated whether the relationship of EVs and the *mrpA*-containing amplicon was restricted to the surface of the vesicles or, if at the same time, these extrachromosomal elements could be protected inside the particles. EVs derived from the WT and Sb2000.1 strains were subjected to a DNase I treatment prior to DNA isolation (Figure S1E) and then subjected to DNA-seq. As shown in Figure S1E, the ~16 kb region containing the *mrpA* gene not only was detected but remained highly enriched in Sb2000.1 EVs after DNase I treatment.

Leishmania EVs serve as an efficient mechanism of gene transfer

Once extrachromosomal amplicon-EV association was confirmed, we explored whether these particles could be involved in intraspecies horizontal gene transfer (HGT) and interspecies gene transfer (IGT) events in promastigotes. We first evaluated the ability of EV-driven HGT to influence recipient cell phenotypes in *L. infantum* strains. To this end, we exposed a Sb-hypersensitive strain of *L. infantum* (*Ldi mrpA*$^{-/-}$) (Douanne et al., 2020b) to EVs released by the *L. infantum* Sb-resistant strain Sb2000.1, by means of three different experimental approaches (Figure S2). We performed Transwell experiments with Sb2000.1 or *Ldi mrpA*$^{-/-}$ promastigotes as EV donor cells, and *Ldi mrpA*$^{-/-}$ were recipient cells. The 0.4 μm pores in the insert membrane prohibit the movement of parasites but permit the diffusion of released EVs from the upper chamber to the lower compartment. No Sb was present in the medium during this process. After 7 days of culture, recipient cells were recovered and submitted to dose-response assays in the presence of increasing concentrations of Sb. As depicted in Figure 3A,

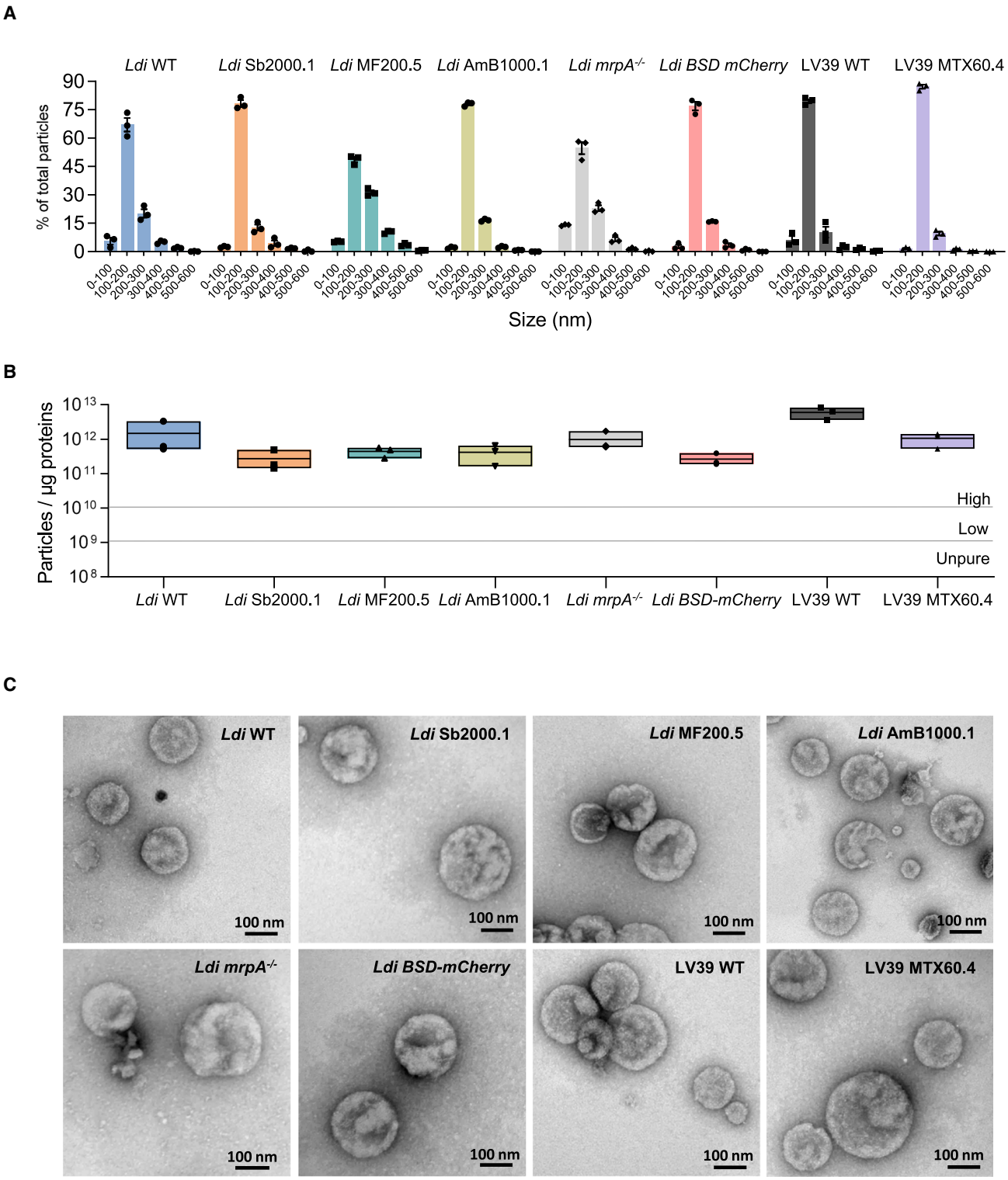

Figure 1. Characterization of EVs released by different *L. infantum* and *L. major* strains used in this study

(A) Particle size distributions obtained by nanoparticle tracking analysis of *Ldi* WT, *Ldi* Sb2000.1, *Ldi* MF200.5, *Ldi* AmB1000.1, *Ldi mrpA*$^{-/-}$, *Ldi-BSD-mCherry*, LV39 WT, and LV39 MTX60.4 strains. Particle size distributions obtained by ZetaView were expressed as percentages after normalization per 10^6 parasites.

(B) Use of particle-to-protein ratio to quantify vesicle purity.

(C) EVs derived from promastigotes were prepared for TEM by negative staining. In (A–C), results are representative of three biological replicates with similar data (or images for the TEM).

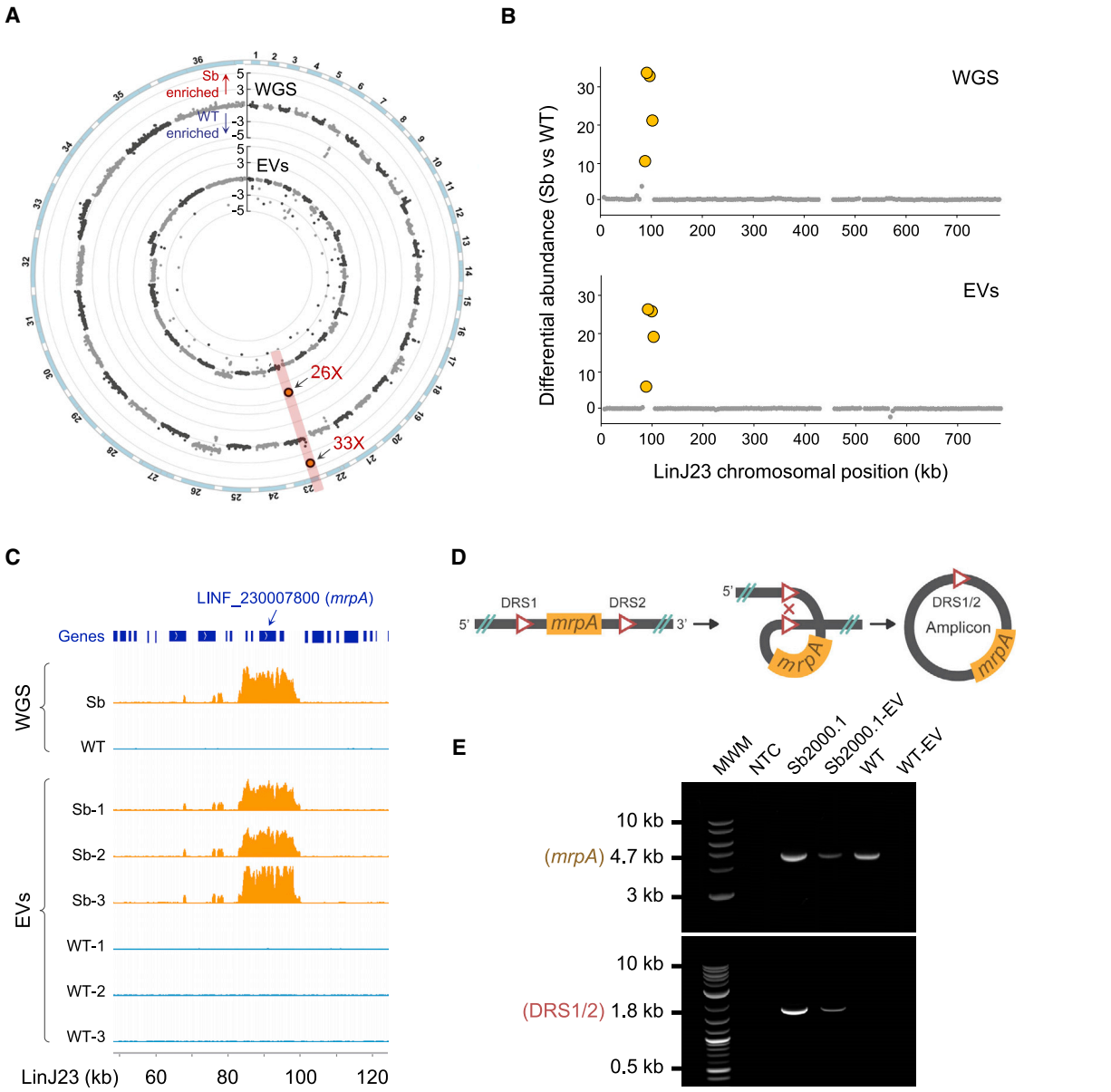

Figure 2. Differential enrichment of EV DNA in Sb-sensitive and Sb-resistant parasites

(A) Circos plot showing the differential abundance between the whole genome (WGS; outer ring) and the EVs (inner ring) comparing Sb-resistant versus WT parasites for each chromosome. The y axis maximum range was set to −5 to +5, with a region on chromosome LinJ23 highlighted in red and with the above axis fold differences indicated.

(B) Miami plots showing the enrichment of a 20 kb genomic window (position 80–100 kb) on LinJ23 in both WGS and EVs.

(C) Sequencing coverage tracks for *L. infantum* WT and Sb2000.1 WGS and triplicates of EVs at the *mrpA* locus; the tracks were normalized according to the total number of mapped reads, read length, and genome size.

(D) Model for the formation of the extrachromosomal circular DNA amplicon on chromosome 23. The amplicon is generated through homologous recombination between the direct repeated sequences (DRS1 and DRS2).

(E) PCR experiments validating the presence of the extrachromosomal circular amplicon (DRS1/2; 1.8 kb) containing the *mrpA* resistance gene (4.7 kb) in the Sb2000.1 drug-resistant strain and its EVs. Results are representative of three biological replicates with similar data.

recipient parasites exposed to Sb2000.1 displayed increased resistance levels compared with those exposed to *Ldi mrpA*$^{-/-}$, with a significant ~2-fold increase in the EC_{50} value (Figure 3B). Moreover, the EC_{50} of *Ldi mrpA*$^{-/-}$ exposed to EVs from *Ldi mrpA*$^{-/-}$ parasites did not change compared with *Ldi mrpA*$^{-/-}$ alone (Table S1). To further confirm whether this phenotypic transformation was directly caused by EVs, we exposed the recipient *Ldi mrpA*$^{-/-}$ strain to purified EVs recovered from Sb2000.1 or *Ldi mrpA*$^{-/-}$ strains (Figure 1) for 5 days, in the absence of Sb pressure. Once again, recipient parasites

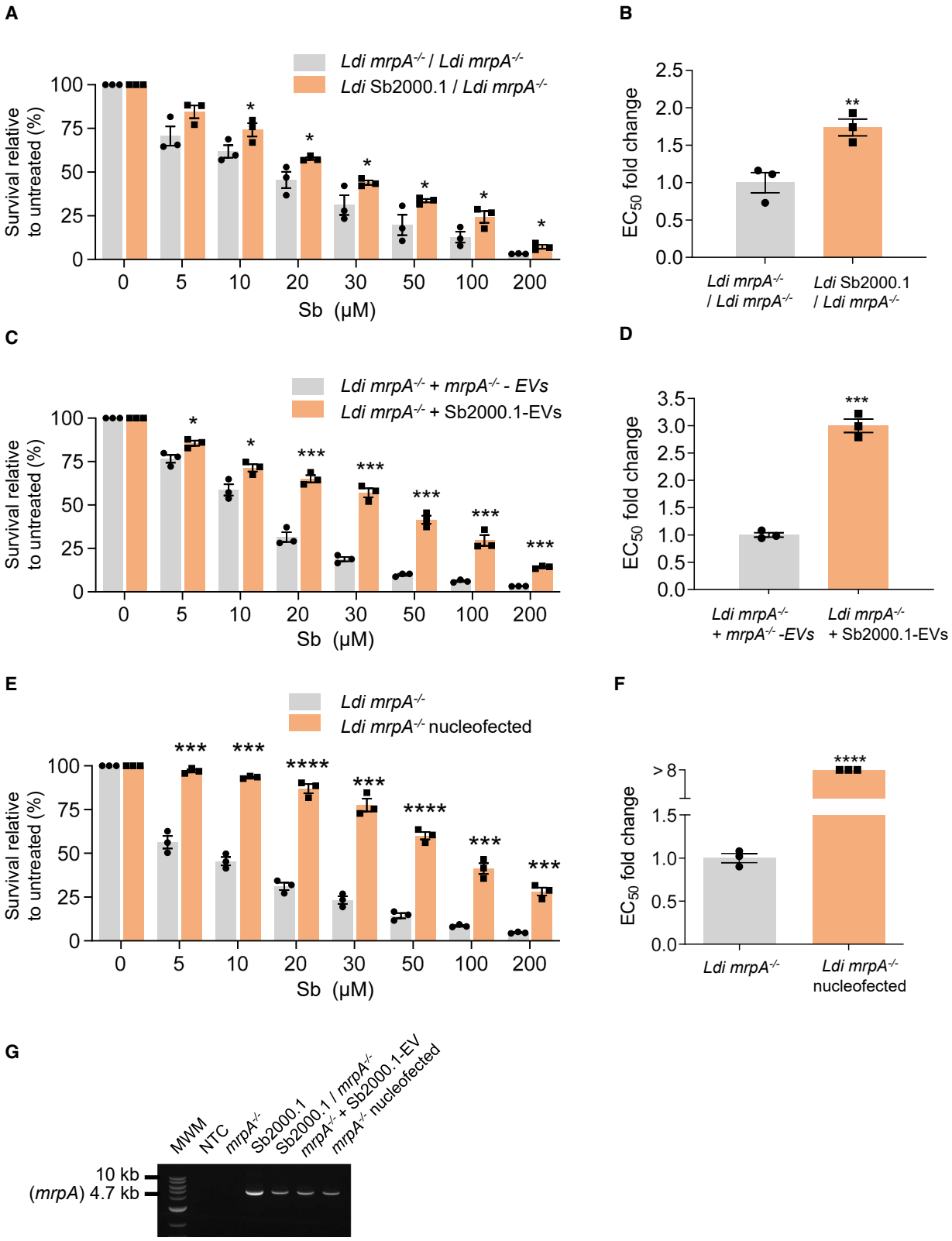

(legend continued on next page)

exposed to Sb2000.1 EVs displayed high levels of resistance to Sb compared with those exposed to their own vesicles (Figure 3C); with a significant ~3-fold shift in EC_{50} value (Figure 3D). For the last approach, drug-resistant EVs were used as the transfection substrate. Once transfected with Sb2000.1 EVs, *Ldi mrpA*$^{-/-}$ recipient parasites were subjected to Sb-drug pressure for one passage (7 days of stabilization) and then tested with dose-response curves. Direct delivery of EV content inside the cell nucleus, coupled with a positive selection, led to high levels of drug resistance in the parasites exposed to Sb2000.1 EVs (Figure 3E), with a >8-fold increase in the EC_{50} (Figure 3F). To further confirm the success of the HGT event, and since the recipient cell line was null for *mrpA*, we proceeded to the extraction of total DNA from recipient parasites after their exposure to EVs and conducted a PCR amplification targeting the complete coding sequence of *mrpA*. As depicted in Figure 3G, PCR led to the amplification of the expected ~4.7 kb product corresponding to the *mrpA* ORF in all three *Ldi mrpA*$^{-/-}$ recipient populations (Transwell, pure EVs, and nucleofection; Figure 3G). To further verify that these findings were not restricted to the *mrpA* null mutant—and assess whether the transferred DNA was being transcribed by the recipient cells—we exposed *Ldi* WT promastigotes to a single dose of WT- or Sb2000.1-purified EVs and recovered the total RNA on the fifth day after exposure. As expected, *mrpA* RNA levels were significantly increased (Figure S3), which supports the drug-resistant phenotype observed after exposure to drug-resistant small EVs.

Next, we explored the potential involvement of EVs in IGT. To this end, we used *L. infantum* (*Ldi*) and *L. major* (*LV39*) WT strains, as well as an *L. major* strain resistant to methotrexate (MTX) (*LV39* MTX60.4), which contains an extrachromosomal circular amplicon (result of a homologous recombination event, as schematized in Figure 4A) comprising the dihydrofolate reductase-thymidylate synthase (*DHFR-TS*) locus, known to be the main target of MTX (Ubeda et al., 2008). First, we conducted a series of PCR experiments targeting the homologous-recombination junction that is present only in the amplicon, and not in the chromosomal sequence. The amplicon signal was detected in the total DNA of only *LV39* MTX60.4, as well as being associated with the vesicles of the MTX-resistant strain (Figure 4B). Naive cultures of both *L. major* WT and *L. infantum* WT parasites were exposed to *LV39* MTX60.4 through Transwell assays, direct exposure to purified EVs, and nucleofection experiments. After Transwell assays, both *L. major* and *L. infantum* recipient parasites showed a significantly enhanced ability to survive in the presence of higher concentrations of MTX (Figure 4C), with an ~1.4-fold shift in their EC_{50} value (Figure 4D). Likewise, recipient parasites exposed to EVs purified from the *LV39* MTX60.4 were also able to better survive in the presence of MTX (Figure 4E), with ~4-fold (*L. major*) and ~2.5-fold (*L. infantum*) increases in their EC_{50} values (Figure 4F). Finally, as previously demonstrated for the *mrpA* amplicon, direct nucleofection of pure EVs led to very high levels of resistance to MTX in both *L. infantum* and *L. major* recipient parasites (Figure 4G), with a >8-fold increase in their EC_{50} value (Figure 4H).

Plasmids containing foreign elements can efficiently propagate through small EVs

We further explored the efficiency of HGT events by using a synthetic plasmid carrying the coding sequences of two different markers: the *mCherry* gene and the blasticidin-resistance gene (*BSD*) (Figure 5A). The *BSD-mCherry* plasmid was transfected as a circular episome in the *L. infantum* WT background, and both parasite DNA and EV DNA were recovered on passage 3 after the transfection. PCR analysis targeting the 399 bp sequence of the *BSD* showed a positive amplification in both total parasite DNA and EV DNA of the novel *Ldi BSD-mCherry* strain (Figure 5B). In this case, because of the presence of these two markers, we were able to evaluate both the impact in terms of blasticidin sensitivity and the success of plasmid transfer by the evaluation of mCherry-derived red fluorescence. As shown with amplicon EV experiments, recipient naive parasites exposed to *Ldi BSD-mCherry* EVs through Transwell assays (Figure 5C), direct contact (Figure 5E), and nucleofection (Figure 5G) increased their capacity to survive in the presence of high concentrations of blasticidin by ~1.5- (Figure 5D), ~3.0- (Figure 5F), and >8-fold (Figure 5H), respectively. All three recipient populations exhibited a positive result when tested for the presence of the *BSD* gene by PCR (Figure S4).

We next evaluated the time required to observe red parasites (i.e., expression of the transferred genes) after the exposure of recipient naive parasites to *BSD-mCherry* purified EVs. As shown in Figure S5, no fluorescence was detected in the initial moments; recipient parasites began to express the mCherry protein around 48 h post-exposure. Signal was greatly increased 96–120 h after initial exposure. Of note, these experiments were conducted in blasticidin-free medium, so no drug pressure was driving the selection of the mCherry subpopulation. Next, we compared the success of transmission of the *BSD-mCherry* plasmid to recipient WT parasites using Transwell assays, purified EVs, and direct transfection of EVs (Figure 6). The efficiency of transfer followed the same order as previously seen in terms of

Figure 3. Demonstration of HGT events leading to the transmission of the *mrpA* amplicon from drug-resistant to drug-sensitive strains of *L. infantum*

(A) Dose-response assays to evaluate the phenotype of recipient parasites after medium sharing in co-culture Transwell assays.
(B) EC_{50} fold-change comparison between conditions depicted in (A).
(C) Dose-response assays in recipient parasites after exposure to purified EVs.
(D) EC_{50} fold-change comparison between conditions depicted in (C).
(E) Dose-response assays in recipient parasites after their nucleofection and selection with purified EVs.
(F) EC_{50} fold-change comparison between conditions depicted in (E). In (A), (C), and (E), percentages of survival were calculated and normalized to the untreated control.
(G) PCR for the demonstration of the presence of the *mrpA* gene in *Ldi mrpA*$^{-/-}$ recipient parasites after Transwell assays (A), exposure to EVs (C), and nucleofection (E). In (A–G), the results are representative of three biological replicates with similar data. Each data point represents the average ± SEM (n = 3). Differences were statistically evaluated by one-tailed unpaired t test (*$p \leq 0.05$, **$p \leq 0.01$, ***$p \leq 0.001$, ****$p \leq 0.0001$).

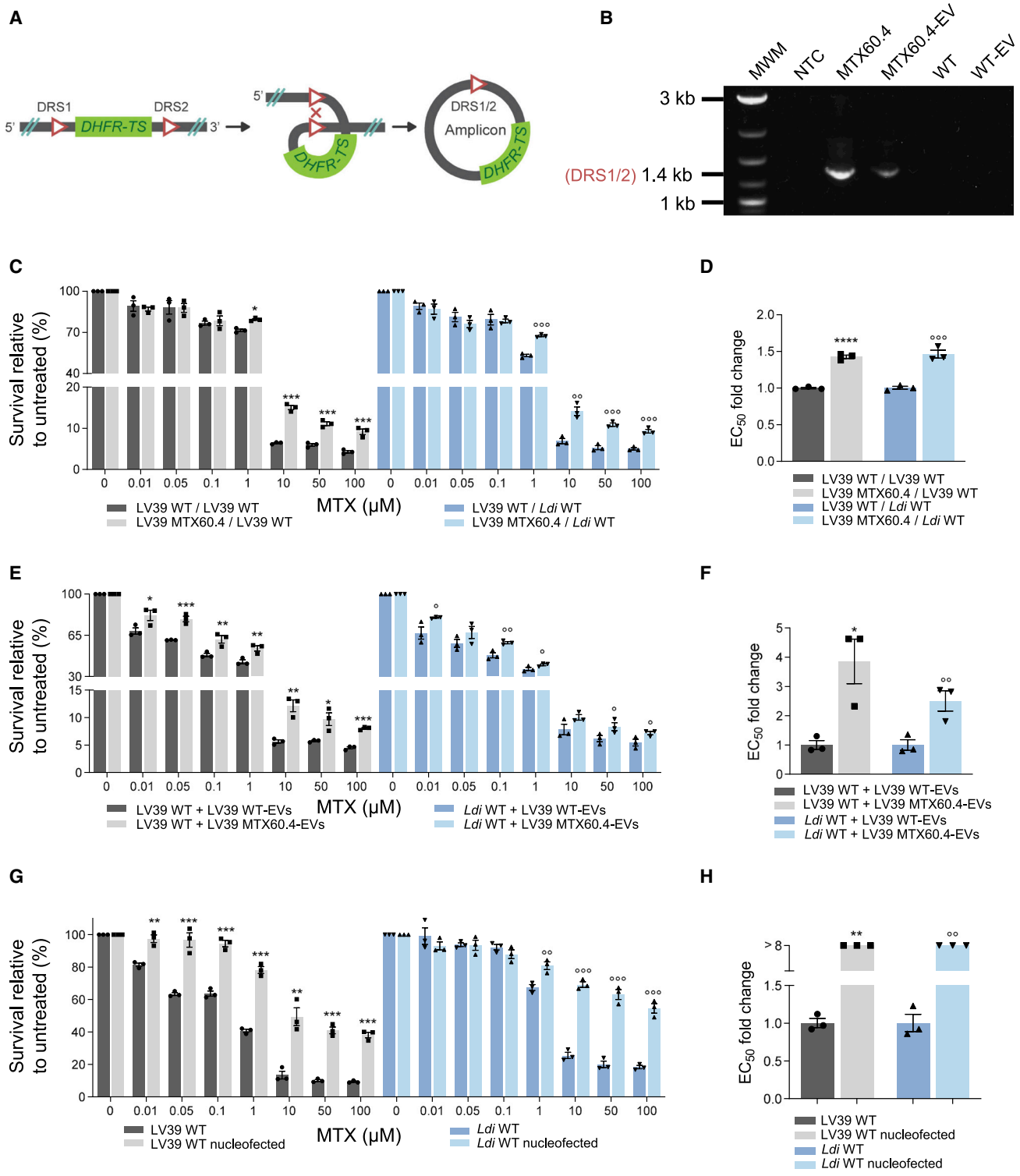

Figure 4. Demonstration of HGT and IGT events leading to the transmission of the *DHFR-TS* circular amplicon from *L. major* drug-resistant parasites to *L. major* and *L. infantum* drug-sensitive strains

(A) Model for the formation of the DHFR-TS circular amplicon.

(B) PCR for the confirmation of the presence of the extrachromosomal *DHFR-TS* circular amplicon (DSR1/2; 1.4 kb) in the LV39 MTX60.4-resistant strain and in its EVs.

(C) Dose-response assays to evaluate the phenotype of recipient parasites after medium sharing in co-culture Transwell assays.

(legend continued on next page)

shift in the EC_{50} values (nucleofection > purified EVs > Transwell). Simultaneous quantification of the total fluorescence signal normalized by the number of parasites showed similar results; with transfer efficiency levels approximately two times higher when using purified EVs (signal corresponding to ~20% of the total population compared with the donor *Ldi BSD-mCherry* strain) than with Transwell assays (~11% of the population) after 120 h of exposure (Figure S6). As expected, nucleofection using purified *BSD-mCherry* EVs resulted in a very strong (~93% of the population) fluorescence phenotype (Figures 6 and S6). Of note, parasites incubated in the presence of the "naked" (no EVs) plasmids did not show any mCherry fluorescence signal (Figures 6 and S6), further supporting the importance of small EVs to guarantee the uptake of the DNA of interest.

EVs released by drug-resistant parasites contribute to reducing cellular stress and stimulate cell proliferation

Using Transwell assays, we evaluated the impact of EVs released by different drug-resistant *Leishmania* strains on the drug cross-sensitivity profiles of naive recipient cells. EVs released by Sb- and AmB-resistant strains caused a reduction in the sensitivity of the WT strain against Sb (Figure 7A). EVs released by the AmB-resistant strain induced a slight but significant reduction in the sensitivity against MF (Figure 7B). Exposure to particles released by the AmB- and MF-resistant strains resulted in decreased sensitivity against AmB (Figure 7C). We next studied the accumulation of reactive oxygen species (ROS) upon drug exposure and the impact of EVs in this process. To this end, *L. infantum*-sensitive parasites were exposed to the EC_{90} of Sb, MF, and AmB in the presence, or the absence, of purified EVs released by the WT, Sb2000.1, MF200.5, and AmB1000.1 strains (Figure 7D). Detection of dichlorofluorescein diacetate (DCFDA) fluorescence confirmed lower levels of ROS production/accumulation in WT promastigotes exposed to EVs derived from drug-resistant strains compared with unexposed parasites. EVs released by the WT did not confer any protection against ROS. As expected, protection against ROS translated into significantly higher survival rates in promastigotes exposed to EVs released by drug-resistant parasites (Figure 7D). Next, we evaluated the impact of EVs released by the WT and the drug-resistant strains on the growth pattern of drug-sensitive parasites in the absence (Figure 7E) or presence of drug-induced stress (Figures 7F and 7H). EVs released by drug-resistant parasites, but not those of the WT, significantly increased the growth of sensitive recipient parasites (Figure 7E). Moreover, Sb2000.1- and AmB1000.1-derived EVs fostered a greater growth of WT parasites under drug pressure (Figures 7F and 7H, respectively). On the other hand, the effect of MF-derived EVs on parasite growth, while significant, was milder and transient (Figure 7G).

Finally, to better understand the differences in terms of cell growth, we explored potential changes in the proteome of *Ldi* WT recipient promastigotes after 120 h exposure to Sb-resistant *Leishmania* EVs compared with the WT's own EVs. Shotgun proteomics revealed four proteins detected in the whole-parasite proteome of only the three replicates of WT parasites exposed to Sb-resistant EVs and not in all three replicates exposed to WT-EV (Figures S7A and S6C and Data S2). Among these unique proteins found in the parasites, we identified two dehydrogenase proteins, one involved in the oxidation of malate to oxaloacetate (A4I9I4_LEIIN) and one involved in succinate converting to fumarate (A4HWJ7_LEIIN). In addition, we identified a putative Peter Pan protein (A4HRX6_LEIIN), which could be involved in cellular division and cell-cycle progression. On the other hand, as summarized in the volcano plot (Figure S7B), we identified 17 upregulated ($p < 0.05$; fold change ≥ 2) and 4 downregulated proteins ($p < 0.05$; fold change ≤ 0.5). Among the enriched proteins (Figure S7C) in WT parasites exposed to Sb2000.1 EVs, we identified an enoyl-CoA hydratase (E9AHU0_LEIIN), a farnesyl pyrophosphate synthase (E9AH04_LEIIN), a member of the endosomal sorting complexes required for transport (ESCRT) pathway VPS23 (A4I7R5_LEIIN), and a dynein-associated protein (A4IB75_LEIIN).

DISCUSSION

Drug resistance in *Leishmania* continues to emerge, diversify, and spread (Fernández-Prada et al., 2019). While the effect of antileishmanial drugs on host-infecting amastigotes has been largely studied, interest in the propagation of drug-resistance traits in the sand fly vector has only recently drawn the attention of the scientific community (Van Bockstal et al., 2020). Of note, *Leishmania* can undergo genetic exchange during growth and development in the sand fly vector through cryptic sex. However, the occurrence of viable hybrid offspring is variable depending on the experimental conditions (Akopyants et al., 2009; Louradour et al., 2020, 2022; Monte-Neto et al., 2022). Alternatively, acquisition of genes via HGT in the vector would represent an efficient and less challenging mechanism of genetic exchange by facilitating a rapid genome diversification. However, such a mechanism had never been described in eukaryotic parasites before. Moreover, and to guarantee efficient HGT, DNA should be protected from degradation during its cell-to-cell transit. In this way, we recently showed that *Leishmania* EVs are naturally secreted in the vector (Atayde et al., 2015), and they serve as an envelope for LRV1 virions (Atayde et al., 2019). This points to EVs as potential shuttles for nucleic acid transfer in *Leishmania*.

The first question we addressed in this work was the potential occurrence of specific leishmanial DNA associated with EVs,

(D) EC_{50} fold-change comparison between conditions depicted in (C).
(E) Dose-response assays in recipient parasites after exposure to purified EVs.
(F) EC_{50} fold-change comparison between conditions depicted in (E).
(G) Dose-response assays in recipient parasites after their nucleofection and selection with purified EVs.
(H) EC_{50} fold-change comparison between conditions depicted in (G). In (C), (E), and (G), percentages of survival were calculated and normalized to the untreated control. In (B–H), the results are representative of three biological replicates with similar data. Each data point represents the average ± SEM (n = 3). Differences were statistically evaluated by one-tailed unpaired t test ($^{*/o}p \leq 0.05$, $^{**/oo}p \leq 0.01$, $^{***/ooo}p \leq 0.001$).

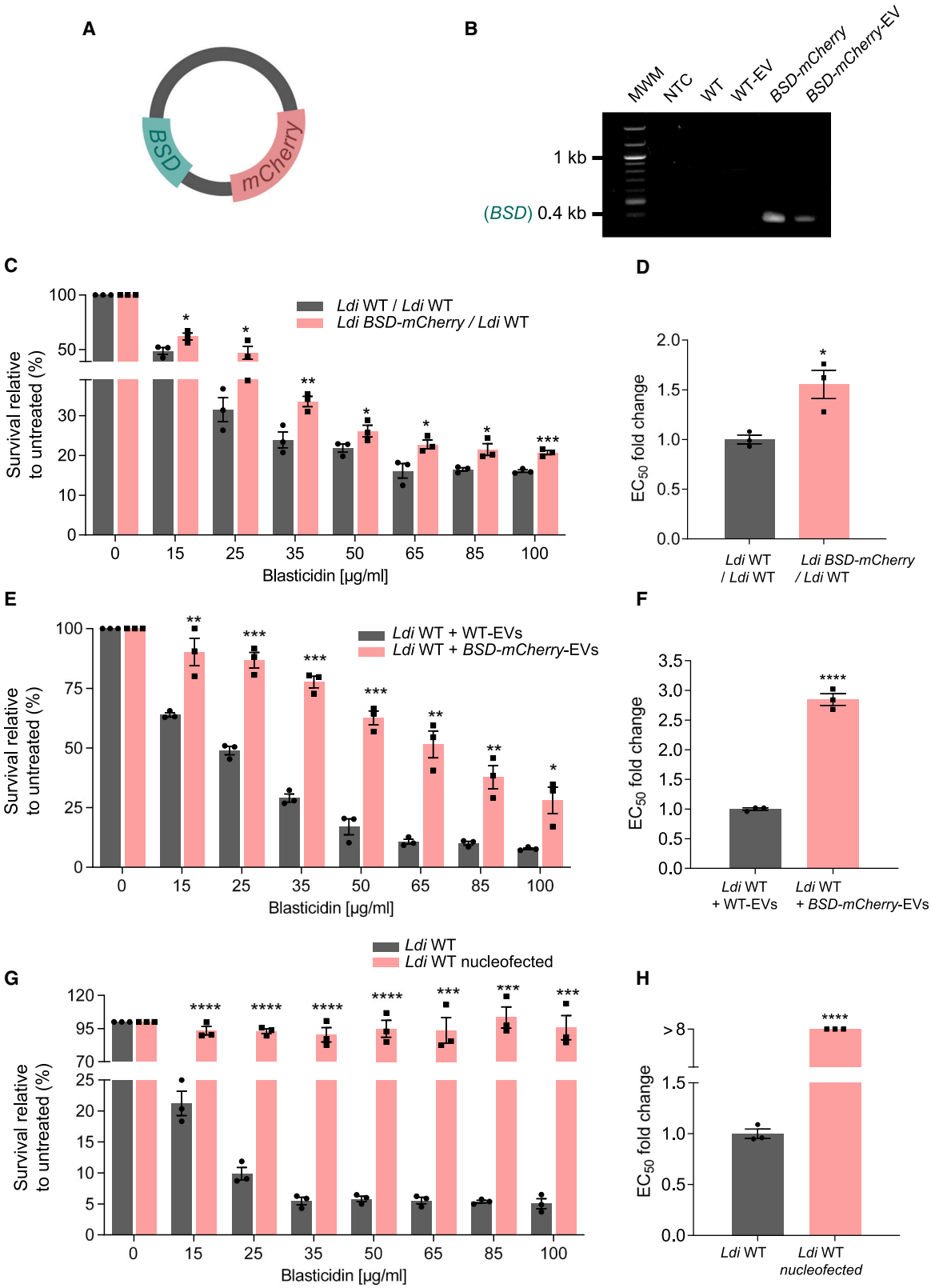

(legend on next page)

and whether this EV DNA could vary depending on the drug-resistance background of the parasite. Numerous studies have reported the presence of DNA both attached to the surface of tumor-derived EVs and in their lumen (Elzanowska et al., 2021). Likewise, a recent metagenomic study showed the presence of antibiotic-resistance genes in bacterial EVs in indoor dust (Qin et al., 2022). Our EV DNA-seq experiments revealed that fragments from almost the entire genome of *L. infantum* WT and Sb2000.1 strains were represented in their respective small EVs. EV-DNA genomic fragments could represent a highly diverse source of gene CNVs, which are a well-established mechanism of genetic adaption in *Leishmania* (Leprohon et al., 2015). Indeed, when encountering a stressor (i.e., drug pressure or physical stress such as temperature), the subset of parasites with increased CNVs—leading to increased expression of genes involved in countering the challenge—would survive. Of note, EV-driven CNVs could contribute to a rapid genetic diversification of the population in the sand fly vector, as well as inducing rapid fitness gains to effectively respond to environmental signals and stressors in the absence of regulated transcription (Grünebast and Clos, 2020). Likewise, tumor-derived EVs are known to contain double-stranded genomic DNA spanning all chromosomes (reflecting the genetic status of the tumor, i.e., single-nucleotide polymorphisms [SNPs] and CNVs) (Balaj et al., 2011; Kahlert et al., 2014; Vagner et al., 2018) and could potentially participate in the process of cancer metastasis and drug resistance (Zhang et al., 2018). Our analyses pinpointed a major enrichment of EV DNA corresponding to the region encoding the *mrpA* gene on chromosome LinJ23, reflecting the genetic background of the Sb2000.1 strain (Leprohon et al., 2009), and thus pointing to a potential transfer of resistance. Of note, the presence of the *mrpA* amplicon was not restricted to the exofacial surface of Sb2000.1 EVs, given that the same amplification was detected by DNA-seq after DNase treatment. This, in fact, could confer increased stability to the amplicon by protecting it from the external environment during an HGT event. Due to their size, small EVs (<200 nm) can transport a limited amount of material in their lumen. However, the presence of dsDNA fragments ranging from 100 bp to 20 kb has been confirmed in small EVs (i.e., exosomes) released by tumor cells (Kahlert et al., 2014; Lee et al., 2016), further substantiating our findings of an ~16 kb *mrpA* amplification in *Leishmania* EVs. That said, the mechanism of DNA packaging in uptake by EVs remains unclear (Elzanowska et al., 2021). During each mitotic division the nucleus disassembles and re-forms, releasing nuclear content into the cytoplasm. Since the ESCRT pathway participates in both membrane abscission during cytokinesis and regeneration of the nuclear envelope (Stoten and Carlton, 2018), this could represent the most favorable moment for amplicon uptake by *Leishmania* EVs.

Next, we demonstrated, through three different approaches, that EVs released by drug-resistant parasites can efficiently alter the drug-sensitivity phenotype of recipient parasites after a single exposure, through the transmission of natural amplicons (i.e., *mrpA* and *DHFR* genes) or artificial plasmids (i.e., *BSD*). Moreover, this observation was conserved, and gene transfers were functional between visceral and cutaneous leishmaniasis species as demonstrated by MTX-resistance transfer from *L. major* MTX60.4 to *L. infantum* parasites. Likewise, genomic exchange through interspecies-hybrid formation has been recently reported both *in vitro* and in the sand fly vector (Louradour et al., 2022; Romano et al., 2014). Importantly, we showed that, when exposing naive parasites to purified drug-resistant EVs, levels of drug sensitivity in the recipient cells were increased by 2- to 3-fold after a single exposure. While less efficient, continuous exposure in Transwell co-culture experiments also led to a significant decrease in drug sensitivity in recipient parasites. Similarly, Pereira and co-workers showed that co-culture of Sb-resistant and Sb-sensitive *Leishmania* strains recovered from patients resulted in an improvement in growth capacity and an increased resistance of sensitive parasites (Pereira et al., 2021). While they did not identify the mechanism underlying these phenotypic changes, their observational results further reinforce our mechanistic findings. In addition, this could have major clinical implications: increased EC_{50} values will translate to poor, or even ineffective, treatment response in leishmaniasis patients (Pereira et al., 2021).

Our most striking evidence of HGT events was the demonstration of the efficient transfer of the extrachromosomally amplified genes *mrpA* and *BSD* into the naive background of recipient *mrpA*$^{-/-}$ and WT *L. infantum* strains after exposure to donor EVs. While a few reports have recently described the gene transfer potential of outer membrane vesicles (OMVs) of Gram-negative bacteria (Dell'Annunziata et al., 2021), we now demonstrate HGT in eukaryotic parasites through EVs. While leishmanial amplicons share some similarities with prokaryotic plasmids (i.e., circular architecture and multi-gene content), *Leishmania* extrachromosomal DNAs do not include any genetic factor known to facilitate their transfer among parasites (Beverley, 1991). However, this evolutionary limitation could have been circumvented by EVs, which, as supported by our findings, would facilitate the diffusion of genetic elements to surrounding parasites, as we also showed previously for LRV1 (Atayde et al., 2019). In addition to being a very efficient source of genetic diversity, EV DNA

Figure 5. Demonstration of HGT events leading to the transmission of artificial plasmid containing *BSD* and *mCherry* genes

(A) Schematic representation of the pLEXY-*BSD-mCherry* plasmid.

(B) PCR confirmation of the presence of the pLEXY-*BSD-mCherry* (*BSD* gene) in *L. infantum BSD-mCherry* and its vesicles.

(C) Dose-response assays to evaluate the phenotype of recipient parasites after medium sharing in co-culture Transwell assays.

(D) EC_{50} fold-change comparison between conditions depicted in (C).

(E) Dose-response assays in recipient parasites after exposure to purified EVs.

(F) EC_{50} fold-change comparison between conditions depicted in (E).

(G) Dose-response assays in recipient parasites after their nucleofection and selection with purified EVs.

(H) EC_{50} fold-change comparison between conditions depicted in (G). In (C), (E), and (G), percentages of survival were calculated and normalized to the untreated control. Each data point represents the average ± SE (n = 3 biological replicates). Differences were statistically evaluated by one-tailed unpaired t test (*$p \leq 0.05$, **$p \leq 0.01$, ***$p \leq 0.001$, ****$p \leq 0.0001$).

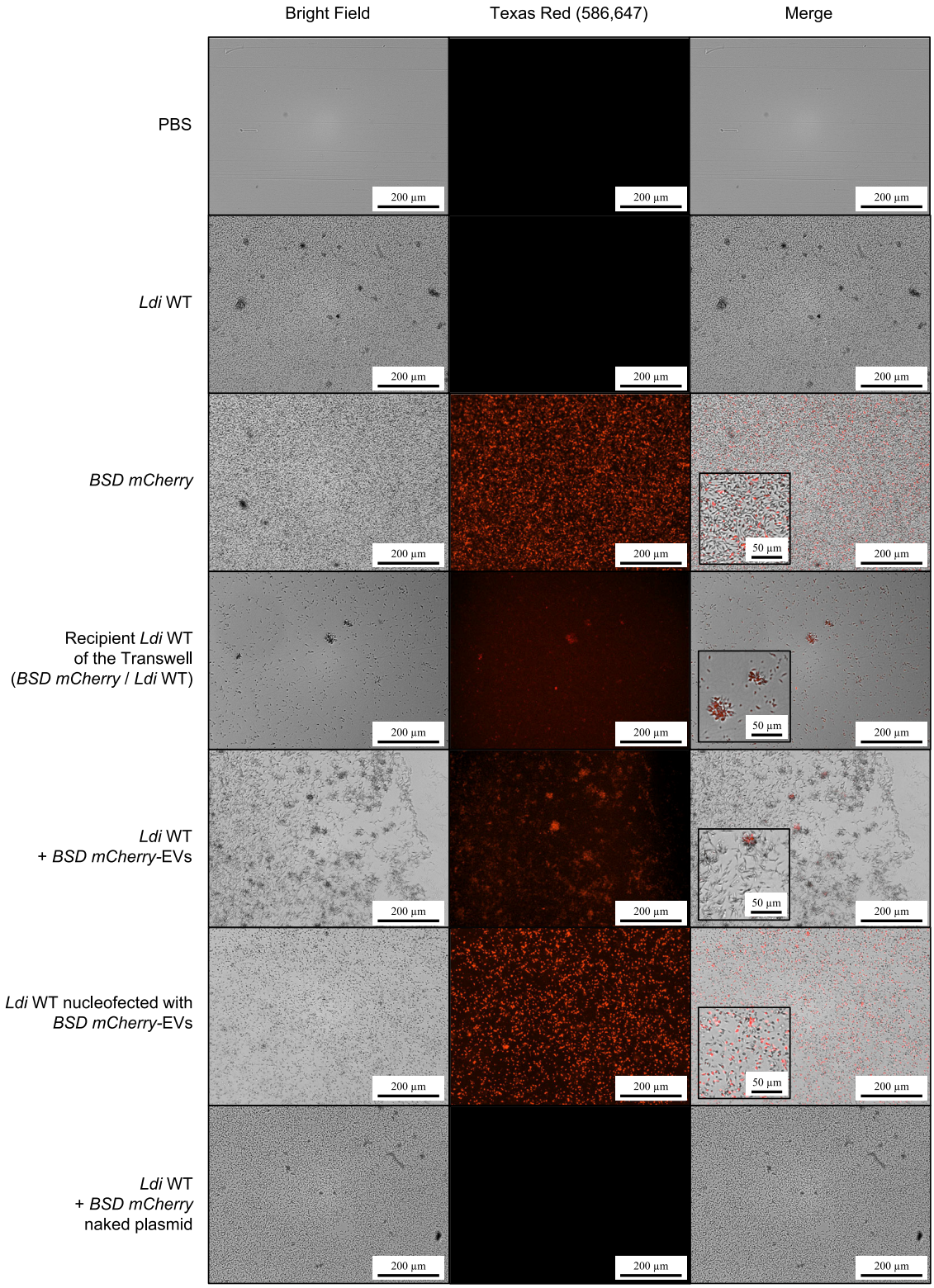

Figure 6. Detection of mCherry signal by fluorescence microscopy in naive recipient parasites after exposure to *BSD-mCherrry*-EVs

Promastigotes (10^7) corresponding to each strain/condition were washed and plated in black 24-well plates with flat and clear bottom for high-throughput microscopy. Microscopy images were captured with a Cytation 5 machine (BioTek) equipped with the Texas red filter cube (ex/em 586/647 nm). The results are representative of three biological replicates with similar data.

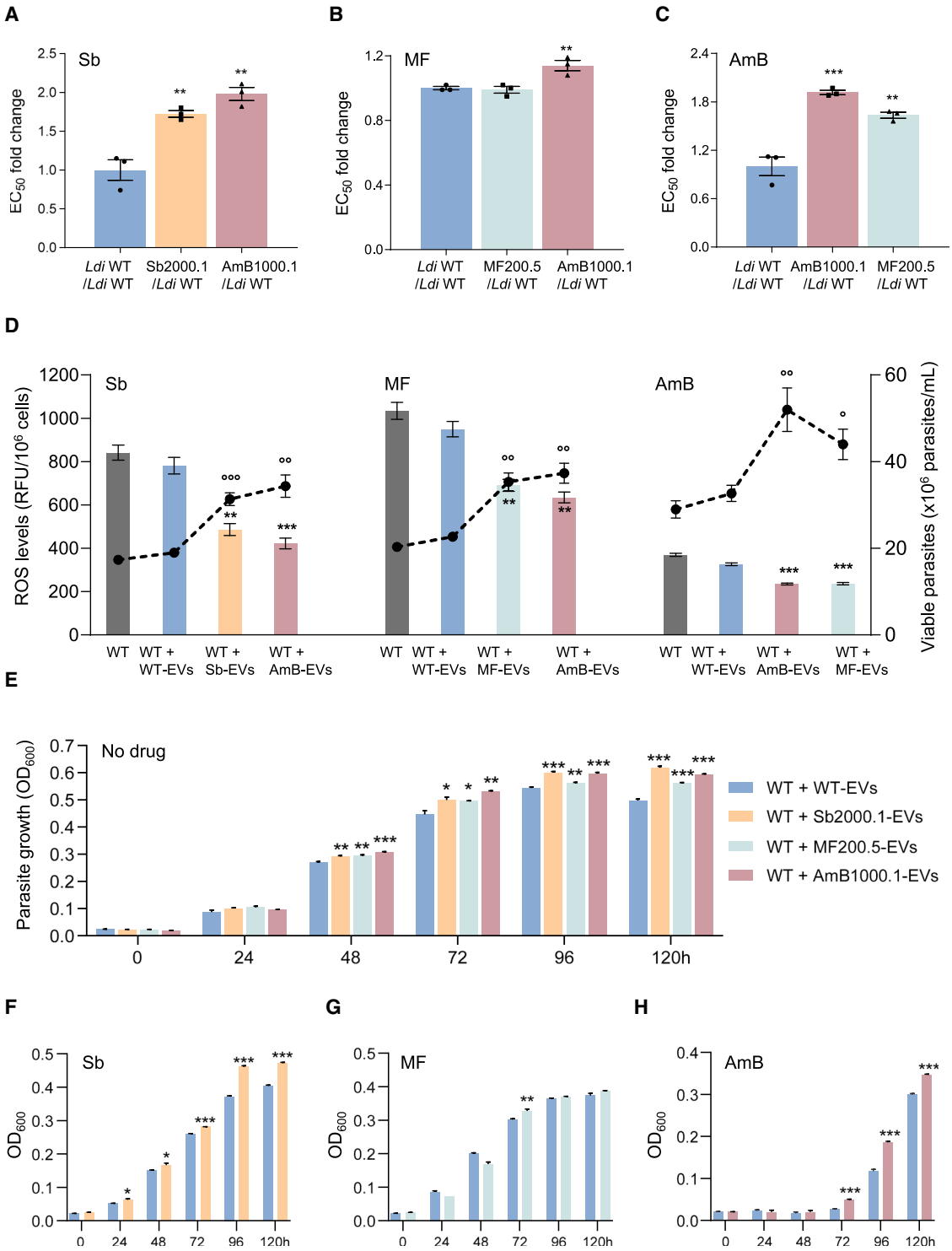

Figure 7. Evaluation of the impact of drug-resistant EVs on the drug-sensitivity profile, control of ROS, and general fitness of WT drug-sensitive parasites

(A–C) Evaluation of phenotypic changes (EC_{50} fold change) in *L. infantum* WT sensitive parasites after 7 days of medium sharing (Transwell assays) with Sb2000.1, MF200.5, and AmB1000.1 *L. infantum* drug-resistant strains.

(D) Measurement of drug-induced (Sb, MF, and AmB) ROS accumulation (DCFDA fluorescence; Cytation 5; ex/em 485/535 nm) in *L. infantum* WT cells in the presence or absence of purified EVs (WT or drug resistant). Graphs represents the number of viable promastigotes normalized to 10^6 cells/mL (points) and DCFDA fluorescence normalized to 10^6 promastigotes (bars).

(legend continued on next page)

could represent a safekeeping mechanism by acting as a highly diverse library of DNA "repair templates" (i.e., for correcting harmful homozygous mutations or irreversible deletions) shared between parasites within the sand fly vector. On the other hand, this new EV-driven genetic-exchange mechanism implies that drug resistance could spread in sand fly populations, even in the absence of drug pressure.

Expression of proteins encoded by EV-transferred genes took up to 72 h, as per detection of mCherry reporter fluorescence emission. This delay in detection further corroborates the transmission of *mCherry* DNA, rather than the protein, and sheds some light on the time required for the release of EV-DNA cargo into the cytoplasm of recipient parasites and subsequent intracellular trafficking to their nucleus. To this extent, different studies have shown that plasmids use the microtubule network and the retrograde motor dynein to reach the cell nucleus after transfection in eukaryotic cells (Vaughan and Dean, 2006). Likewise, our proteomic analyses revealed a significant enrichment in dynein-associated proteins in parasites exposed to EVs containing drug-resistance amplicons (i.e., WT exposed to Sb2000.1 EVs for 120 h). However, further studies are needed to better understand DNA vesicular absorption mechanisms. In addition, we showed that EV-mediated genetic-exchange events could be efficient in *Leishmania*, as a single exposure to EVs led to a transformation of ~20% of the population in the absence of any selection pressure. This HGT efficiency rate is comparable to that reported in *L. major-L. major* hybrid selection experiments (7%–26%) in the sand fly vector (Akopyants et al., 2009; Monte-Neto et al., 2022). Whether both mechanisms are linked should be addressed in future studies.

To succeed through its parasitic life cycle, resistance-conferring genetic alterations must guarantee the survival of the parasite under stressors not only in the mammalian host but also inside the sand fly vector (Van Bockstal et al., 2020). Several reports have shown that drug-resistant *Leishmania* parasites are more tolerant when exposed to different stressors (i.e., starvation, heat shock-pH stress, etc.) (Berg et al., 2015). Thus, we explored the potential involvement of EVs released by donor drug-resistant parasites in the modulation of redox control and tolerance to stress in naive recipient parasites. To this end, we verified potential mechanisms of cross-resistance when exposing sensitive recipient parasites to EVs issued by parasites resistant to the three main antileishmanial drugs. We confirmed a cross-resistant phenotype between AmB and MF (Fernandez-Prada et al., 2016) previously reported, and we pinpointed a previously unknown cross-resistance to Sb when parasites were exposed to AmB1000.1 EVs. This could be explained by the enrichment of AmB1000.1 EVs with MRPA protein, as described in our previous EV proteomics studies (Douanne et al., 2020a). Of note, we showed that WT receiving EVs from drug-resistant parasites were able to grow better and survive for longer in a non-drugged environment. Increased growth rate was coupled to a better tolerance toward, or reduced production of, ROS when parasites were exposed to high concentrations of various antileishmanial drugs. This enhanced ability to neutralize drug-induced ROS production was not transferred by WT EVs, which is in line with previous metabolomic studies showing that drug-resistant parasites are protected against drug-induced oxidative stress as part of a general adaptation mechanism that is independent of the drug toward which the parasite has become resistant (Berg et al., 2015).

Next, we explored the potential reprogramming of *Leishmania*'s proteome during its stationary phase (fifth day of growth) after an initial, single-dose exposure to EVs released by drug-resistant parasites. Patterns of protein expression of recipient parasites exposed to EVs changed according to the drug-resistance background of the donor cell. Among the proteins detected only in parasites exposed to Sb2000.1 EVs, we identified succinate and malate dehydrogenases, both known to be potentially involved in promastigote growth and metacyclogenesis. Succinate dehydrogenase (mitochondrial complex II) may be of particular importance, as succinate is the main trypanosomatid respiratory substrate (Verner et al., 2014). In eukaryotic cells, complex II can be a source as well as a suppressor of ROS, and its processes are highly linked to the tricarboxylic acid (TCA) cycle. Among TCA-cycle intermediates, oxaloacetate (a product of malate dehydrogenase) can efficiently inhibit complex II and minimize superoxide production (Dröse, 2013). This could explain the protective effect of Sb-resistant EVs against ROS formation, as well as the enhanced growth observed in recipient parasites. Likewise, enrichment in enoyl-CoA hydratase and farnesyl pyrophosphate synthase could translate into enhanced growth, as these are two key intermediates in the biosynthesis of all isoprenoids, which are precursors of many end-products that are essential for cell viability. Farnesyl pyrophosphate is used by trypanosomatids in the biosynthesis of dolichol and sterols, such as ergosterol, and in protein prenylation (Gadelha et al., 2020). Finally, the presence of VPS23 protein, belonging to ESCRT-II, coupled to the enrichment of a dynein-associated protein could reflect an increased rate of cellular division, as vesiculation contributes to membrane abscission during cytokinesis (Stoten and Carlton, 2018). Future work should address the functionality (i.e., enzymatic activity) of these altered pathways and further elucidate the signaling cascade leading to their enrichment in naive parasites after exposure to drug-resistant EVs.

Collectively, our study reveals that *Leishmania* parasites exploit EVs to guarantee the propagation of drug-resistance genes as part of episomal amplifications, which constitutes a demonstration of EV-mediated HGT in eukaryotic parasites, as well as an alternative mechanism of drug resistance in eukaryotic cells. In addition, EVs derived from drug-resistant parasites modulate promastigote fitness by reducing the accumulation of ROS, when encountering stressors, and altering the basal proteome of recipient parasites, further guaranteeing the survival and propagation of drug-resistant populations.

(E) Parasite growth in the presence of purified EVs was measured (Cytation 5; OD_{600}) every 24 h for 6 days in drug-free media.
(F–H) Parasite growth in the presence of purified EVs was measured (Cytation 5; OD_{600}) every 24 h for 6 days in medium containing Sb, MF, or AmB. In (A–H), the results are representative of three biological replicates with similar data. Each data point represents the average ± SEM. Differences were statistically evaluated by one-tailed unpaired t test ($^{*/o}p \leq 0.05$, $^{**/oo}p \leq 0.01$, $^{***/ooo}p \leq 0.001$).

Limitations of the study

DNA is not restricted to the nucleus in eukaryotic cells, as these also possess a mitochondrial genome. Mitochondrial DNA (mtDNA) can be released to the extracellular space as cell-free mtDNA in association with EVs. The *Ldi* WT reference genome assembly does not include the kinetoplast DNA (mtDNA, or kDNA); hence, our analyses focused on the nuclear DNA, which contains the known drug-resistance genes. Further studies are also needed to elucidate the intracellular processes involved in packaging DNA into *Leishmania* EVs, and whether DNA structure and intracellular origin have a role in this process. Moreover, while we have proved the link between drug-resistance genes transferred through EVs (i.e., *mrpA*, *dhfr*, and *BSD*) and changes in the phenotype (i.e., decreased drug sensitivity) of recipient cells, EVs could contain molecules other than DNA (i.e., different thiol species) that could be contributing to survival against off-target or non-specific stressors (i.e., cross-resistance through increased protection against ROS). Finally, it also remains to be determined how the HGT and IGT mechanisms proposed here will apply to other eukaryotic organisms under different physiological and stressful conditions.

STAR★METHODS

Detailed methods are provided in the online version of this paper and include the following:

- KEY RESOURCES TABLE
- RESOURCE AVAILABILITY
  - Lead contact
  - Materials availability
  - Data and code availability
- EXPERIMENTAL MODEL AND SUBJECT DETAILS
  - *Leishmania* cell lines
- METHOD DETAILS
  - Drug sensitivity assays
  - *Leishmania* growth experiments
  - Generation of the *L. infantum BSD-mCherry* strain
  - Isolation and purification of *Leishmania* small EVs
  - Small EVs size and concentration measurements
  - Transmission electron microscopy (TEM)
  - Isolation of DNA from whole promastigotes and purified small EVs
  - DNA amplification and visualization
  - DNA sequencing and analysis
  - Transfer of EV-associated DNA
  - Measurement of reactive oxygen species (ROS) accumulation
  - LC–MS/MS
  - Database searching and protein identification
  - Proteomics analysis
- QUANTIFICATION AND STATISTICAL ANALYSIS

SUPPLEMENTAL INFORMATION

Supplemental information can be found online at https://doi.org/10.1016/j.celrep.2022.111121.

ACKNOWLEDGMENTS

The authors want to thank Prof. Marc Ouellette for the kind gift of the *L. infantum* Sb2000.1, MF200.5, AmB1000.1, and *L. major* MTX60.4 drug-resistant strains. We also thank Dr. Aida Mínguez-Menéndez for her help with the creation of scientific figures. This work was supported by a Canada Institutes of Health Research (CIHR) Project Grant (#173450) to C.F.-P. and M.O. C.F.-P. was also supported by the Canada Foundation for Innovation (CFI) John R. Evans Leaders Fund (#37324 and #38858). D.L. was supported by a CIHR Project Grant (#168959). D.L. was also supported by an FRQ-S, Chercheur-Boursier Junior 1 Award and by the CFI John R. Evans Leaders Fund. N.D. and G.D. were respectively supported by the Fonds de recherche du Québec – Nature et technologies (FRQNT) and the CIHR studentship programs.

AUTHOR CONTRIBUTIONS

Conceptualization, N.D., M.O., and C.F.P.; methodology, N.D., G.D., A.A., M.B., D.L., M.O., and C.F.P.; investigation, N.D., G.D., A.A., and L.B.; formal analysis, N.D., G.D., A.A., D.L., and C.F.P.; writing – original draft, N.D. and C.F.P.; writing – review & editing, D.L., M.O., and C.F.P.; visualization, N.D., G.D., A.A., D.L., and C.F.P.; supervision, M.B., D.L., M.O., and C.F.P.; resources, D.L., M.O., and C.F.P.; funding acquisition, M.O. and C.F.P.

DECLARATION OF INTERESTS

All authors declare no competing interests.

Received: April 21, 2022
Revised: June 2, 2022
Accepted: June 29, 2022
Published: July 19, 2022

REFERENCES

Akopyants, N.S., Kimblin, N., Secundino, N., Patrick, R., Peters, N., Lawyer, P., Dobson, D.E., Beverley, S.M., and Sacks, D.L. (2009). Demonstration of genetic exchange during cyclical development of *Leishmania* in the sand fly vector. Science *324*, 265–268. https://doi.org/10.1126/science.1169464.

Andrews, S. (2010). FastQC: A Quality Control Tool for High Throughput Sequence Data. [Online]. https://www.bioinformatics.babraham.ac.uk/projects/fastqc/.

Aslett, M., Aurrecoechea, C., Berriman, M., Brestelli, J., Brunk, B.P., Carrington, M., Depledge, D.P., Fischer, S., Gajria, B., Gao, X., et al. (2010). TriTrypDB: a functional genomic resource for the Trypanosomatidae. Nucleic Acids Res. *38*, D457–D462. https://doi.org/10.1093/nar/gkp851.

Atayde, V., Aslan, H., Townsend, S., Hassani, K., Kamhawi, S., and Olivier, M. (2015). Exosome secretion by the parasitic Protozoan *Leishmania* within the sand fly midgut. Cell Rep. *13*, 957–967. https://doi.org/10.1016/j.celrep.2015.09.058.

Atayde, V.D., da Silva Lira Filho, A., Chaparro, V., Zimmermann, A., Martel, C., Jaramillo, M., and Olivier, M. (2019). Exploitation of the *Leishmania* exosomal pathway by Leishmania RNA virus 1. Nat. Microbiol. *4*, 714–723. https://doi.org/10.1038/s41564-018-0352-y.

Balaj, L., Lessard, R., Dai, L., Cho, Y.J., Pomeroy, S.L., Breakefield, X.O., and Skog, J. (2011). Tumour microvesicles contain retrotransposon elements and amplified oncogene sequences. Nat. Commun. *2*, 180. https://doi.org/10.1038/ncomms1180.

Bellotti, C., Lang, K., Kuplennik, N., Sosnik, A., and Steinfeld, R. (2021). High-grade extracellular vesicles preparation by combined size-exclusion and affinity chromatography. Sci. Rep. *11*, 10550. https://doi.org/10.1038/s41598-021-90022-y.

Berg, M., García-Hernández, R., Cuypers, B., Vanaerschot, M., Manzano, J.I., Poveda, J.A., Ferragut, J.A., Castanys, S., Dujardin, J.C., and Gamarro, F. (2015). Experimental resistance to drug combinations in *Leishmania donovani*:

metabolic and phenotypic adaptations. Antimicrob. Agents Chemother. *59*, 2242–2255. https://doi.org/10.1128/AAC.04231-14.

Beverley, S.M. (1991). Gene amplification in *Leishmania*. Annu. Rev. Microbiol. *45*, 417–444. https://doi.org/10.1146/annurev.mi.45.100191.002221.

Bolger, A.M., Lohse, M., and Usadel, B. (2014). Trimmomatic: a flexible trimmer for Illumina sequence data. Bioinformatics *30*, 2114–2120. https://doi.org/10.1093/bioinformatics/btu170.

Brotherton, M.C., Bourassa, S., Leprohon, P., Légaré, D., Poirier, G.G., Droit, A., and Ouellette, M. (2013). Proteomic and genomic analyses of antimony resistant *Leishmania infantum* mutant. PLoS One *8*, e81899. https://doi.org/10.1371/journal.pone.0081899.

Brotherton, M.C., Bourassa, S., Légaré, D., Poirier, G.G., Droit, A., and Ouellette, M. (2014). Quantitative proteomic analysis of amphotericin B resistance in *Leishmania infantum*. Int. J. Parasitol. Drugs Drug Resist. *4*, 126–132. https://doi.org/10.1016/j.ijpddr.2014.05.002.

Bussotti, G., Gouzelou, E., Côrtes Boité, M., Kherachi, I., Harrat, Z., Eddaikra, N., Mottram, J.C., Antoniou, M., Christodoulou, V., Bali, A., et al. (2018). *Leishmania* genome dynamics during environmental adaptation reveal strain-specific differences in gene copy number variation, karyotype instability, and telomeric amplification. mBio *9*. e01399–18. https://doi.org/10.1128/mBio.01399-18.

Calvo-Álvarez, E., Álvarez-Velilla, R., Jiménez, M., Molina, R., Pérez-Pertejo, Y., Balaña-Fouce, R., and Reguera, R.M. (2014). First evidence of intraclonal genetic exchange in trypanosomatids using two *Leishmania infantum* fluorescent transgenic clones. PLoS Negl. Trop. Dis. *8*, e3075. https://doi.org/10.1371/journal.pntd.0003075.

da Silva Lira Filho, A., Fajardo, E.F., Chang, K.P., Clément, P., and Olivier, M. (2022). Leishmania exosomes/extracellular vesicles containing GP63 are essential for enhance cutaneous leishmaniasis development upon Co-inoculation of *Leishmania amazonensis* and its exosomes. Front. Cell. Infect. Microbiol. *11*, 709258. https://doi.org/10.3389/fcimb.2021.709258.

Dell'Annunziata, F., Folliero, V., Giugliano, R., De Filippis, A., Santarcangelo, C., Izzo, V., Daglia, M., Galdiero, M., Arciola, C.R., and Franci, G. (2021). Gene transfer potential of outer membrane vesicles of gram-negative bacteria. Int. J. Mol. Sci. *22*, 5985. https://doi.org/10.3390/ijms22115985.

Dey, R., Joshi, A.B., Oliveira, F., Pereira, L., Guimarães-Costa, A.B., Serafim, T.D., de Castro, W., Coutinho-Abreu, I.V., Bhattacharya, P., Townsend, S., et al. (2018). Gut microbes egested during bites of infected sand flies augment severity of leishmaniasis via inflammasome-derived IL-1β. Cell Host Microbe *23*, 134–143.e6. https://doi.org/10.1016/j.chom.2017.12.002.

Dong, G., Wagner, V., Minguez-Menendez, A., Fernandez-Prada, C., and Olivier, M. (2021). Extracellular vesicles and leishmaniasis: current knowledge and promising avenues for future development. Mol. Immunol. *135*, 73–83. https://doi.org/10.1016/j.molimm.2021.04.003.

Douanne, N., Dong, G., Douanne, M., Olivier, M., and Fernandez-Prada, C. (2020a). Unravelling the proteomic signature of extracellular vesicles released by drug-resistant *Leishmania infantum* parasites. PLoS Negl. Trop. Dis. *14*, e0008439. https://doi.org/10.1371/journal.pntd.0008439.

Douanne, N., Wagner, V., Roy, G., Leprohon, P., Ouellette, M., and Fernandez-Prada, C. (2020b). MRPA-independent mechanisms of antimony resistance in *Leishmania infantum*. Int. J. Parasitol. Drugs Drug Resist. *13*, 28–37. https://doi.org/10.1016/j.ijpddr.2020.03.003.

Downing, T., Imamura, H., Decuypere, S., Clark, T.G., Coombs, G.H., Cotton, J.A., Hilley, J.D., de Doncker, S., Maes, I., Mottram, J.C., et al. (2011). Whole genome sequencing of multiple *Leishmania donovani* clinical isolates provides insights into population structure and mechanisms of drug resistance. Genome Res. *21*, 2143–2156. https://doi.org/10.1101/gr.123430.111.

Dröse, S. (2013). Differential effects of complex II on mitochondrial ROS production and their relation to cardioprotective pre- and postconditioning. Biochim. Biophys. Acta *1827*, 578–587. https://doi.org/10.1016/j.bbabio.2013.01.004.

El Fadili, K., Messier, N., Leprohon, P., Roy, G., Guimond, C., Trudel, N., Saravia, N.G., Papadopoulou, B., Legare, D., and Ouellette, M. (2005). Role of the ABC transporter MRPA (PGPA) in antimony resistance in *Leishmania infantum* axenic and intracellular amastigotes. Antimicrob. Agents Chemother. *49*, 1988–1993. https://doi.org/10.1128/AAC.49.5.1988-1993.2005.

Elzanowska, J., Semira, C., and Costa-Silva, B. (2021). DNA in extracellular vesicles: biological and clinical aspects. Mol. Oncol. *15*, 1701–1714. https://doi.org/10.1002/1878-0261.12777.

Fernandez-Prada, C., Vincent, I.M., Brotherton, M.C., Roberts, M., Roy, G., Rivas, L., Leprohon, P., Smith, T.K., and Ouellette, M. (2016). Different mutations in a P-type ATPase transporter in *Leishmania* parasites are associated with cross-resistance to two leading drugs by distinct mechanisms. PLoS Negl. Trop. Dis. *10*, e0005171. https://doi.org/10.1371/journal.pntd.0005171.

Fernández-Prada, C., Douanne, N., Minguez-Menendez, A., Pena, J., Tunes, L.G., Pires, D.E.V., and Monte-Neto, R.L. (2019). Repurposed molecules: a new hope in tackling neglected infectious diseases. In In Silico Drug Design, K. Roy, ed. (Academic Press), pp. 119–160. https://doi.org/10.1016/B978-0-12-816125-8.00005-5.

Gadelha, A.P.R., Brigagao, C.M., da Silva, M.B., Rodrigues, A.B.M., Guimarães, A.C.R., Paiva, F., de Souza, W., and Henriques, C. (2020). Insights about the structure of farnesyl diphosphate synthase (FPPS) and the activity of bisphosphonates on the proliferation and ultrastructure of *Leishmania* and *Giardia*. Parasit. Vectors *13*, 168. https://doi.org/10.1186/s13071-020-04019-z.

García-Alcalde, F., Okonechnikov, K., Carbonell, J., Cruz, L.M., Götz, S., Tarazona, S., Dopazo, J., Meyer, T.F., and Conesa, A. (2012). Qualimap: evaluating next-generation sequencing alignment data. Bioinformatics *28*, 2678–2679. https://doi.org/10.1093/bioinformatics/bts503.

Gotz, S., Garcia-Gomez, J.M., Terol, J., Williams, T.D., Nagaraj, S.H., Nueda, M.J., Robles, M., Talon, M., Dopazo, J., and Conesa, A. (2008). High-throughput functional annotation and data mining with the Blast2GO suite. Nucleic Acids Res. *36*, 3420–3435. https://doi.org/10.1093/nar/gkn176.

Grünebast, J., and Clos, J. (2020). *Leishmania*: responding to environmental signals and challenges without regulated transcription. Comput. Struct. Biotechnol. J. *18*, 4016–4023. https://doi.org/10.1016/j.csbj.2020.11.058.

Guimond, C., Trudel, N., Brochu, C., Marquis, N., El Fadili, A., Peytavi, R., Briand, G., Richard, D., Messier, N., Papadopoulou, B., et al. (2003). Modulation of gene expression in *Leishmania* drug resistant mutants as determined by targeted DNA microarrays. Nucleic Acids Res. *31*, 5886–5896. https://doi.org/10.1093/nar/gkg806.

Hassani, K., Shio, M.T., Martel, C., Faubert, D., and Olivier, M. (2014). Absence of metalloprotease GP63 alters the protein content of *Leishmania* exosomes. PLoS One *9*, e95007. https://doi.org/10.1371/journal.pone.0095007.

Kahlert, C., Melo, S.A., Protopopov, A., Tang, J., Seth, S., Koch, M., Zhang, J., Weitz, J., Chin, L., Futreal, A., and Kalluri, R. (2014). Identification of double-stranded genomic DNA spanning all chromosomes with mutated KRAS and p53 DNA in the serum exosomes of patients with pancreatic cancer. J. Biol. Chem. *289*, 3869–3875. https://doi.org/10.1074/jbc.C113.532267.

Langdon, W.B. (2015). Performance of genetic programming optimised Bowtie2 on genome comparison and analytic testing (GCAT) benchmarks. BioData Min. *8*, 1. https://doi.org/10.1186/s13040-014-0034-0.

Lee, T.H., Chennakrishnaiah, S., Meehan, B., Montermini, L., Garnier, D., D'Asti, E., Hou, W., Magnus, N., Gayden, T., Jabado, N., et al. (2016). Barriers to horizontal cell transformation by extracellular vesicles containing oncogenic H-ras. Oncotarget *7*, 51991–52002. https://doi.org/10.18632/oncotarget.10627.

Leprohon, P., Legare, D., Raymond, F., Madore, E., Hardiman, G., Corbeil, J., and Ouellette, M. (2009). Gene expression modulation is associated with gene amplification, supernumerary chromosomes and chromosome loss in antimony-resistant *Leishmania infantum*. Nucleic Acids Res. *37*, 1387–1399. https://doi.org/10.1093/nar/gkn1069.

Leprohon, P., Fernandez-Prada, C., Gazanion, É., Monte-Neto, R., and Ouellette, M. (2015). Drug resistance analysis by next generation sequencing in *Leishmania*. Int. J. Parasitol. Drugs Drug Resist. *5*, 26–35. https://doi.org/10.1016/j.ijpddr.2014.09.005.

Li, H. (2013). Aligning sequence reads, clone sequences and assembly contigs with BWA-MEM. Preprint at arXiv. 1303.3997.

Li, H., Handsaker, B., Wysoker, A., Fennell, T., Ruan, J., Homer, N., Marth, G., Abecasis, G., and Durbin, R.; 1000 Genome Project Data Processing Subgroup (2009). The sequence alignment/map format and SAMtools. Bioinformatics *25*, 2078–2079. https://doi.org/10.1093/bioinformatics/btp352.

Liao, Y., Smyth, G.K., and Shi, W. (2014). featureCounts: an efficient general purpose program for assigning sequence reads to genomic features. Bioinformatics *30*, 923–930. https://doi.org/10.1093/bioinformatics/btt656.

Louradour, I., Ferreira, T.R., Ghosh, K., Shaik, J., and Sacks, D. (2020). In vitro generation of Leishmania hybrids. Cell Rep. *31*, 107507. https://doi.org/10.1016/j.celrep.2020.03.071.

Louradour, I., Ferreira, T.R., Duge, E., Karunaweera, N., Paun, A., and Sacks, D. (2022). Stress conditions promote *Leishmania* hybridization in vitro marked by expression of the ancestral gamete fusogen HAP2 as revealed by single-cell RNA-seq. Elife *11*, e73488. https://doi.org/10.7554/eLife.73488.

Monte-Neto, R.L., Fernandez-Prada, C., and Moretti, N.S. (2022). Sex under pressure: stress facilitates *Leishmania in vitro* hybridization. Trends Parasitol. *38*, 274–276. https://doi.org/10.1016/j.pt.2022.02.001.

Moreira, W., Leprohon, P., and Ouellette, M. (2011). Tolerance to drug-induced cell death favours the acquisition of multidrug resistance in *Leishmania*. Cell Death Dis. *2*, e201. https://doi.org/10.1038/cddis.2011.83.

Mukherjee, A., Padmanabhan, P.K., Singh, S., Roy, G., Girard, I., Chatterjee, M., Ouellette, M., and Madhubala, R. (2007). Role of ABC transporter MRPA, gamma-glutamylcysteine synthetase and ornithine decarboxylase in natural antimony-resistant isolates of *Leishmania donovani*. J. Antimicrob. Chemother. *59*, 204–211. https://doi.org/10.1093/jac/dkl494.

Pereira, L.O.R., Sousa, C.S., Ramos, H.C.P., Torres-Santos, E.C., Pinheiro, L.S., Alves, M.R., Cuervo, P., Romero, G.A.S., Boité, M.C., Porrozzi, R., and Cupolillo, E. (2021). Insights from *Leishmania (Viannia) guyanensis in vitro* behavior and intercellular communication. Parasit. Vectors *14*, 556. https://doi.org/10.1186/s13071-021-05057-x.

Picard, T. (2018). http://broadinstitute.github.io/picard/.

Qin, Y., Guo, Z., Huang, H., Zhu, L., Dong, S., Zhu, Y.G., Cui, L., and Huang, Q. (2022). Widespread of potential pathogen-derived extracellular vesicles carrying antibiotic resistance genes in indoor dust. Environ. Sci. Technol. *56*, 5653–5663. https://doi.org/10.1021/acs.est.1c08654.

Ramírez, F., Ryan, D.P., Grüning, B., Bhardwaj, V., Kilpert, F., Richter, A.S., Heyne, S., Dündar, F., and Manke, T. (2016). deepTools2: a next generation web server for deep-sequencing data analysis. Nucleic Acids Res. *44*, W160–W165. https://doi.org/10.1093/nar/gkw257.

Robinson, M.D., McCarthy, D.J., and Smyth, G.K. (2010). edgeR: a Bioconductor package for differential expression analysis of digital gene expression data. Bioinformatics *26*, 139–140. https://doi.org/10.1093/bioinformatics/btp616.

Robinson, J.T., Thorvaldsdóttir, H., Winckler, W., Guttman, M., Lander, E.S., Getz, G., and Mesirov, J.P. (2011). Integrative genomics viewer. Nat. Biotechnol. *29*, 24–26. https://doi.org/10.1038/nbt.1754.

Romano, A., Inbar, E., Debrabant, A., Charmoy, M., Lawyer, P., Ribeiro-Gomes, F., Barhoumi, M., Grigg, M., Shaik, J., Dobson, D., et al. (2014). Cross-species genetic exchange between visceral and cutaneous strains of *Leishmania* in the sand fly vector. Proc. Natl. Acad. Sci. USA *111*, 16808–16813. https://doi.org/10.1073/pnas.1415109111.

Silverman, J.M., Clos, J., de'Oliveira, C.C., Shirvani, O., Fang, Y., Wang, C., Foster, L.J., and Reiner, N.E. (2010). An exosome-based secretion pathway is responsible for protein export from *Leishmania* and communication with macrophages. J. Cell Sci. *123*, 842–852. https://doi.org/10.1242/jcs.056465.

Stoten, C.L., and Carlton, J.G. (2018). ESCRT-dependent control of membrane remodelling during cell division. Semin. Cell Dev. Biol. *74*, 50–65. https://doi.org/10.1016/j.semcdb.2017.08.035.

Sundar, S., and Singh, B. (2018). Emerging therapeutic targets for treatment of leishmaniasis. Expert Opin. Ther. Targets *22*, 467–486. https://doi.org/10.1080/14728222.2018.1472241.

Tripp, C.A., Myler, P.J., and Stuart, K. (1991). A DNA sequence (LD1) which occurs in several genomic organizations in *Leishmania*. Mol. Biochem. Parasitol. *47*, 151–160. https://doi.org/10.1016/0166-6851(91)90174-5.

Ubeda, J.M., Légaré, D., Raymond, F., Ouameur, A., Boisvert, S., Rigault, P., Corbeil, J., Tremblay, M.J., Olivier, M., Papadopoulou, B., and Ouellette, M. (2008). Modulation of gene expression in drug resistant *Leishmania* is associated with gene amplification, gene deletion and chromosome aneuploidy. Genome Biol. *9*, R115. https://doi.org/10.1186/gb-2008-9-7-r115.

Ubeda, J.M., Raymond, F., Mukherjee, A., Plourde, M., Gingras, H., Roy, G., Lapointe, A., Leprohon, P., Papadopoulou, B., Corbeil, J., and Ouellette, M. (2014). Genome-wide stochastic adaptive DNA amplification at direct and inverted DNA repeats in the parasite Leishmania. PLoS Biol. *12*, e1001868. https://doi.org/10.1371/journal.pbio.1001868.

UniProt Consortium (2019). UniProt: a worldwide hub of protein knowledge. Nucleic Acids Res. *47*, D506–D515. https://doi.org/10.1093/nar/gky1049.

Vagner, T., Spinelli, C., Minciacchi, V.R., Balaj, L., Zandian, M., Conley, A., Zijlstra, A., Freeman, M.R., Demichelis, F., De, S., et al. (2018). Large extracellular vesicles carry most of the tumour DNA circulating in prostate cancer patient plasma. J. Extracell. Vesicles *7*, 1505403. https://doi.org/10.1080/20013078.2018.1505403.

Van Bockstal, L., Hendrickx, S., Maes, L., and Caljon, G. (2020). Sand fly studies predict transmission potential of drug-resistant *Leishmania*. Trends Parasitol. *36*, 785–795. https://doi.org/10.1016/j.pt.2020.06.006.

Vaughan, E.E., and Dean, D.A. (2006). Intracellular trafficking of plasmids during transfection is mediated by microtubules. Mol. Ther. *13*, 422–428. https://doi.org/10.1016/j.ymthe.2005.10.004.

Verner, Z., Čermáková, P., Škodová, I., Kováčová, B., Lukeš, J., and Horváth, A. (2014). Comparative analysis of respiratory chain and oxidative phosphorylation in *Leishmania tarentolae, Crithidia fasciculata, Phytomonas serpens* and procyclic stage of Trypanosoma brucei. Mol. Biochem. Parasitol. *193*, 55–65. https://doi.org/10.1016/j.molbiopara.2014.02.003.

Yáñez-Mó, M., Siljander, P.R.M., Andreu, Z., Bedina Zavec, A., Borràs, F.E., Buzas, E.I., Buzas, K., Casal, E., Cappello, F., Carvalho, J., et al. (2015). Biological properties of extracellular vesicles and their physiological functions. J. Extracell. Vesicles *4*, 27066. https://doi.org/10.3402/jev.v4.27066.

Yin, L., Zhang, H., Tang, Z., Xu, J., Yin, D., Zhang, Z., Yuan, X., Zhu, M., Zhao, S., Li, X., and Liu, X. (2021). rMVP: a memory-efficient, visualization-enhanced, and parallel-accelerated tool for genome-wide association study. Genomics Proteomics Bioinformatics *19*, 619–628. https://doi.org/10.1016/j.gpb.2020.10.007.

Zhang, C., Ji, Q., Yang, Y., Li, Q., and Wang, Z. (2018). Exosome: function and role in cancer metastasis and drug resistance. Technol. Cancer Res. Treat. *17*, 153303381876345. https://doi.org/10.1177/1533033818763450.

STAR★METHODS

KEY RESOURCES TABLE

REAGENT or RESOURCE	SOURCE	IDENTIFIER
Chemicals, peptides, and recombinant proteins		
Sb (potassium antimonyl tartrate trihydrate)	Sigma	Cat#383376–100g
Acide borique	Sigma	Cat#10043-35-3
Adenine	Sigma	Cat#A2545-25g
Agarose	Fisher	Cat#BP160-500
AmB (amphotericin B solution)	Sigma	Cat#A2942-100mL
Ammonium bicarbonate	Fisher	Cat#1066-33-7
Ampicillin	Sigma	Cat#A9518-25g
BSD (blasticidin S hydrochloride)	Gibco	Cat#R210-01
CAN (Ceric Ammonium Nitrate)	Fisher	Cat#RDCC0300500
H2DCFDA (H2-DCF, DCF)	Invitrogen, USA	Cat# D399
DNAzol reagent	Invitrogen, USA	Cat#10503027
DTT (dithiothreitol)	Thermo Fisher Scientific, USA	Cat#R0861
EDTA (Ethylenediaminetetraacetic acid)	Sigma	Cat#60-00-4
FBS	Wisent	Cat#80150
Formic acid	Sigma	Cat#64-18-6
Glucose	Gibco	Cat#A2494001
Glutaraldehyde solution	Fisher	Cat# BP25471
Hemin Chloride	MP Biomedicals	Cat#194025
HEPES	Sigma	Cat#H4034-500g
Kanamycin	Sigma	Cat#K4000-25g
KCl	Fisher	Cat#AC418205000
M199 medium	Gibco	Cat#31100–019
MTF (miltefosine)	Cayman Chem. cie	Cat#63280
MOPS	Sigma	Cat#M3183
MTX (methotrexate hydrate)	Sigma	Cat#A6770-25mg
$Na_2HPO_47H_20$ (phosphate sodium dibasique anhydre)	Fisher	Cat#7558-79-4
NaCl	Fisher	Cat#AA1101930
$NaHC0_3$ (Sodium Bicarbonate)	VWR	Cat#BDH0280-2,5Kg
Puromycin solution 10 mg/mL	Wisent	Cat# 450-162-XL
RPMI-1640 1X medium (with L-glutamine, without HEPES & phenol red)	Wisent	Cat#250-046-CL
Sodium cacodylate	Fisher	Cat# AAJ60367AE
SYBR Safe DNA Gel Stain	Invitrogen, USA	Cat#S33102
Trichloroacetic acid (15%)	Fisher	Cat#13-622-625
Tris (1 M), pH 8.0, RNase-free	Invitrogen	Cat#AM9856
Triton X-100	Sigma	Cat#9002-93-1
Uranyl acetate	SPI supplies	Cat#6159-44-0
Critical commercial assays		
DNeasy Blood and Tissue Kit	QIAGEN, USA	Cat#69504
Human T cell Nucleofector Kit	Lonza Bioscience	Cat#VPA-1002
KAPA HyperPrep Kit	Roche	#KK8500
MicroBCA Protein Assay Kit	Thermo Fisher Scientific, USA	Cat#PI23235
Quant-iT Pico Green dsDNA Assay Kit	Thermo Fisher Scientific, USA	#P7589

(*Continued on next page*)

Continued		
REAGENT or RESOURCE	SOURCE	IDENTIFIER
Turbo DNA-free Kit	Thermo Fisher Scientific, USA	Cat#AM1907
PCR-free Lucigen NxSeq	Lucigen, USA	#14000
Deposited data		
EV-DNA seq data	This paper	GEO: GSE200222
Proteomic data	This paper	iProX PXD034487
Experimental models: Cell lines		
L. infantum WT (MHOM/MA/67/ITMAP-263)	Laboratory of Prof. Marc Ouellette	N/A
L. infantum Sb2000.1	Laboratory of Prof. Marc Ouellette	N/A
L. infantum MF200.5	Laboratory of Prof. Marc Ouellette	N/A
L. infantum AmB1000.1	Laboratory of Prof. Marc Ouellette	N/A
L. infantum mrpA$^{-/-}$	Douanne et al. (2020b)	https://doi.org/10.1016/j.ijpddr.2020.03.003
L. infantum BSD-mCherry	This paper	N/A
L. major WT	Laboratory of Prof. Marc Ouellette	N/A
L. major MTX60.4	Laboratory of Prof. Marc Ouellette	N/A
Oligonucleotides		
Primers for PCR validation experiments, see Table S2	This paper	N/A
Recombinant DNA		
Plasmid: pLEXSY-2 mCherry Hsp70 BSD	Calvo-Álvarez et al. (2014)	https://doi.org/10.1371/journal.pntd.0003075
Software and algorithms		
GraphdPad Prism 8.0 for Windows	GraphPad Software, La Jolla California USA,	https://www.graphpad.com/scientific-software/prism/
Blast2GO 6.0.1	Gotz et al. (2008)	https://doi.org/10.1093/nar/gkn176
Bowtie 2 (Version 2.4.4)	Langdon (2015)	https://doi.org/10.1186/s13040-014-0034-0
BWA-MEM (Version 0.7.17)	Li (2013)	https://doi.org/10.48550/arXiv.1303.3997
CMplot	Yin et al., (2021)	https://doi.org/10.1016/j.gpb.2020.10.007
deepTools (Version 3.5.1)	Ramírez et al., (2016)	https://doi.org/10.1093/nar/gkw257
edgeR	Robinson et al., (2010)	https://doi.org/10.1093/bioinformatics/btp616
FastQC (Version 0.11.9)	Andrews (2010)	http://www.bioinformatics.babraham.ac.uk/projects/fastqc
FeatureCounts (Version Rsubread 2.8.1)	Liao et al., (2014)	https://doi.org/10.1093/bioinformatics/btt656
IGV (2.11.9)	Robinson et al., (2011)	https://doi.org/10.1038/nbt.1754
Picard Tools (Version 2.26.3)	Picard (2018)	http://broadinstitute.github.io/picard/
Qualimap (Version 2.2.2)	García-Alcalde et al., (2012)	https://doi.org/10.1093/bioinformatics/bts503
SAMtools (Version 1.13)	Li et al., (2009)	https://doi.org/10.1093/bioinformatics/btp352
Scaffold 4.9.0	Proteome Software Inc., Portland, USA	https://support.proteomesoftware.com/hc/en-us
Trimmomatic (Version 0.39)	Bolger et al., (2014)	https://doi.org/10.1093/bioinformatics/btu170

RESOURCE AVAILABILITY

Lead contact

Further information and requests for resources and reagents should be directed to and will be fulfilled by the lead contact, Christopher Fernandez-Prada (christopher.fernandez.prada@umontreal.ca).

Materials availability

This study did not generate new unique reagents.

Data and code availability

- EV DNA-seq data have been deposited at GEO (GSE200222) and are publicly available as of the date of publication. The mass spectrometry proteomics data have been deposited to the ProteomeXchange Consortium (http://proteomecentral.

proteomexchange.org) via the iProX partner repository with the dataset identifier PXD034487. Accession numbers are listed in the key resources table.
- This paper does not report original code.
- Any additional information required to reanalyze the data reported in this paper is available from the lead contact upon request.

EXPERIMENTAL MODEL AND SUBJECT DETAILS

Leishmania cell lines

Eight strains belonging to two different *Leishmania* species, *L. infantum* (belonging to the *Leishmania donovani* complex; *Ld*) and *L. major*, were used in this study. *Leishmania infantum* strains included: *L. infantum* (MHOM/MA/67/ITMAP-263) wild-type strain (WT) and the *in vitro* generated resistant mutants Sb2000.1, AmB1000.1 and MF200.5 (Brotherton et al., 2013, 2014; El Fadili et al., 2005; Fernandez-Prada et al., 2016; Leprohon et al., 2009; Moreira et al., 2011), which are resistant to antimony (Sb), amphotericin B (AmB), and miltefosine (MF), respectively. We also included an antimony-hypersensitive strain (*Ldi-mrpA*$^{-/-}$) which lacks the gene encoding the ATP-binding cassette protein MRPA (Douanne et al., 2020b); and a strain overexpressing an episomal plasmid harboring the *mCherry* and *blasticidin*-resistance genes (*BSD-mCherry*). *Leishmania major* strains included: *L. major* LV39 wild-type strain (LV39 WT) and the *in vitro* generated methotrexate (MTX)-resistant mutant LV39 MTX60.4 (Ubeda et al., 2008).

All strains were grown at 25°C in M199 medium supplemented with 10% fetal bovine serum and 5 μg/mL of haemin at pH 7.0. Drug-resistant strains were grown in the presence of the drug for which they were previously selected for resistance (except during DNA-transmission experiments and isolation of EVs): 2 mM Sb (Potassium antimonyl tartrate, Sigma-Aldrich) for Sb2000.1; 200 μM MF (Miltefosine, Cayman Chem.) for MF200.5; 1 μM AmB (Amphotericin B solution, Sigma) for AmB1000.1; 60 μM MTX (Methotrexate, Sigma-Aldrich); 120 μg/mL blasticidin (Blasticidin S hydrochloride, Sigma-Aldrich) for *Ldi BSD-mCherry*; and 100 μg/mL puromycin (Puromycin dihydrochloride, Wisent) for *Ldi mrpA*$^{-/-}$.

METHOD DETAILS

Drug sensitivity assays

Antileishmanial values were determined by monitoring the growth of promastigotes after 72 h of incubation at 25°C in the presence of increasing drug concentrations of Sb, MF, AmB, MTX, or blasticidin, by measuring A_{600} using a Cytation 5 machine (BioTek, USA). EC_{50} values were calculated based on dose-response curves analyzed by non-linear regression with GraphPad Prism 8.0 software (GraphPad Software, La Jolla California, USA). An average of at least three independent biological replicates run in triplicate was performed for each determination. Before proceeding to purification of EVs, the different strains were analyzed in terms of drug sensitivity to confirm their previously reported phenotypes (Table S1).

Leishmania growth experiments

Growth curves were performed in 25 cm^2 cell culture flasks by seeding 1 × 10^6 parasites/mL, and parasite growth was determined daily, up to 5 days, by measuring A_{600} using a Cytation 5 machine (BioTek, USA). Depending on the experimental conditions, parasites were exposed (5 μg EVs/mL) or not to purified small EVs in the presence or in the absence of the different antileishmanial drugs mentioned above (0 × or 1 × EC_{50}). Growth assays were performed with at least three biological replicates from independent cultures, each of which included three technical replicates.

Generation of the *L. infantum BSD-mCherry* strain

The *BSD-mCherry* overexpressing mutant was generated by introducing the pLEXSY-*mCherry* plasmid in the *L. infantum* strain background as previously described (Calvo-Álvarez et al., 2014). Briefly, for episomal expression, a total of 20 μg of the circular pLEXSY-*BSD-mCherry* plasmid were transfected into *L. infantum* WT parasites by nucleofection using the Amaxa Nucleofector System (Lonza) customized for the Human T cell Nucleofector Kit (U-033 pre-set program). Selection was achieved in the presence of 120 μg/mL blasticidin S (Blasticidin S hydrochloride, Sigma-Aldrich). The phenotype of the resulting mutant was verified by both blasticidin drug-susceptibility tests and fluorescence microscopy (Texas Red Fluorescence Imaging (586–647 nm), Cytation 5 machine (BioTek, USA)).

Isolation and purification of *Leishmania* small EVs

Leishmania small EVs were isolated and purified as we previously described (Atayde et al., 2019; Douanne et al., 2020a). Briefly, 1 L of *Leishmania* parasites (2.5–5.0 × 10^6 parasites/mL) was grown in drug-free M199 at 25°C (supplemented with 10% FBS and 5 μg/mL of haemin at pH 7.0) and left to divide in 10 non-ventilated 75 cm^2 culture flasks (Corning, USA) until they reached late-log phase. Next, parasites were washed twice in PBS and resuspended in 5 mL RPMI-1640 medium (no FBS, no phenol red) (Life Technologies) at a final concentration of 2.5–5.0 × 10^8 parasites/mL, in non-ventilated 25 cm^2 culture flasks (Corning, USA) at 37°C. Parasites were stimulated for 4 h at 37°C to maximize the release of EVs in the medium (Atayde et al., 2019; Douanne et al., 2020a). The viability of parasites was evaluated by propidium-iodide (PI) staining before and after incubation at 37°C. Only cultures with a viability >95.0%

were submitted to subsequent EV-purification steps. After the 4-h incubation, samples were centrifuged 10 min at 3 000 g to eliminate parasites and 10 min at 8,500 g to clear out debris, followed by two subsequent filtrations using 0.45 and 0.22 μm syringe filters. EVs were then recovered by a 1 h ultracentrifugation at 100,000 g using 17 mL polypropylene tubes (16 × 96 mm) in an SW 32 Ti Swinging-Bucket Rotor (Beckman Coulter, USA) and resuspended in EVs buffer (137 mM NaCl, 20 mM HEPES, pH 7.5). EV protein content was determined using the Micro BCA Protein Assay Kit (Pierce Biotechnology, USA) as per the manufacturer's recommendations. EVs were conserved in aliquots in EVs buffer at −80°C for subsequent experiments. Aliquots were slowly thawed on ice before being used (EVs were never refrozen). A minimum of three independent purifications were performed for each strain.

Small EVs size and concentration measurements

Size and concentration measurements of the purified EV samples were performed with a ZetaView Nanoparticle tracking analyzer (NTA) (Particle Metrix, USA). The samples were run at 25°C using 0.22 μm filtered EVs buffer as a diluent. For video acquisition, a shutter frame rate of 45 was used and the sensitivity was set at 85, according to the system's software guidance algorithms. Before measurements were taken, accuracy of the ZetaView was verified using 100 nm standard beads. Samples were diluted in EVs buffer with a dilution factor of 1:1,000–1:10,000 to achieve a particle count in the range of 1,000–2,000.

Transmission electron microscopy (TEM)

TEM visualization of *Leishmania* small EVs was performed in accordance with our previously published method (Douanne et al., 2020a). Briefly, purified EVs were coated on formvar carbon grids, fixed with 1% glutaraldehyde in 0.1 M sodium cacodylate buffer for 1 min, and stained with 1% uranyl acetate for 1 min. A FEI Tecnai 12 120 kV transmission electron microscope was then used for recording the formvar grids coated with the purified EVs. The resulting images were captured with the AMT XR-80C CCD Camera System (Facility for Electron Microscopy Research, McGill University).

Isolation of DNA from whole promastigotes and purified small EVs

Genomic DNAs were prepared from mid-log phase clonal cultures of promastigotes of each strain using DNAzol reagent (Invitrogen, USA), as recommended by the manufacturer. DNA was extracted using the DNeasy Blood and Tissue Kit (QIAGEN, USA) from (i) purified EVs, or (ii) purified EVs after treatment with Turbo DNA-free (Thermo Fisher Scientific, USA), following the manufacturer's instructions, to eliminate external DNA. Dried DNA pellets were resuspended in ddH_2O and further concentrated using a Savant DNA SpeedVac Concentrator (Thermo Electron Corporation, USA). Purified DNAs were fluorometrically quantified using the Quant-iT PicoGreen dsDNA Assay Kit (Thermo Fisher Scientific, USA) in a Take 3 platform (BioTek, USA). DNA was stored at −20 °C until use in subsequent next generation sequencing or PCR experiments.

DNA amplification and visualization

DNA targets (e.g., drug-resistance markers) were amplified from genomic DNA or small-EV associated DNA using compatible primer pairs (Table S2) in a ProFlex PCR System (Applied Biosystems, USA). PCR products were electrophoretically resolved in 1 × TBE, 0.6% agarose gels stained with SYBR™ Safe DNA Gel Stain (Invitrogen, USA). Images were captured using a ChemiDoc MP Imaging System (BioRad, USA).

DNA sequencing and analysis

Extracellular vesicle DNA libraries were constructed using the KAPA HyperPrep kit following the manufacturer's protocol without fragmentation; the final library fragment size was 250–400 bp. Sequencing was performed using an Illumina NovaSeq 6000 sequencer in a 50 bp pair-end configuration. An average 29-fold and 32-fold genome coverage was achieved for the EV DNA samples from the WT and the Sb-resistant mutant, respectively. Whole-genome DNA sequencing (WGS) libraries were prepared from genomic DNA with fragments >40 kbp, using the PCR-free Lucigen NxSeq library kit; the average library fragment size distribution was between 500 and 2,500bp. The WGS libraries were sequenced on an Illumina NovaSeq 6000 in a PE 100bp configuration, and a genome coverage of 208-fold and 27-fold was obtained for the WT and the Sb resistant mutant, respectively. Quality control analysis of the raw sequence reads was performed using FASTQC. Adapters and low-quality bases were trimmed by Trimmomatic (Bolger et al., 2014). Trimmed EV DNA sequences were mapped onto the *Leishmania infantum* reference genome assembly (LINF GCA_900500625.2) using the short-read aligner Bowtie2 (Langdon, 2015) using default parameters. For the WGS alignment, BWA-MEM was used with the default parameter, which supports the alignment of longer Illumina sequences ranging from 70 to 100bp (Li, 2013). Quality of mapping was analyzed using Qualimap (García-Alcalde et al., 2012) and reads with low mapping quality score (MAPQ $\leq$2) were removed using Samtools (Li et al., 2009). PCR duplicates in EV DNA libraries were flagged and removed using Picard. Coverage tracks for the visualization in Integrated Genome Viewer (IGV) were created using deepTools (Ramirez et al., 2016), where the scaling factors were calculated using the following formula: genome size/(mapped read pairs * read length).

For the analysis of copy number variation (CNV), read depth coverage was calculated for 5-kb non-overlapping genomic windows tilling the 36 chromosomes using featureCounts (Liao et al., 2014). Read depth coverage was normalized based on the library size and the EVs DNA differential abundance analysis was performed using edgeR with exactTest method and Benjamini-Hochberg multiple testing correction (adjusted p value threshold 0.05). Five-kb windows with a minimal coverage of 50 counts per million in at least

three samples were included in the CNV analysis. To visualize the results of the CNV analyses, the circular and linear Miami plots were created using the CMplot package in R 3.5.3.

Transfer of EV-associated DNA

The ability of small EVs to transfer DNA to recipient cells was evaluated using three different approaches (Figure S2). For EVs Transwell co-culture (no contact) assays, donor parasites (2×10^7 promastigotes in 1.5 mL) were added to the 0.4 μm pore-size inside chamber (Corning, USA), while recipient parasites (5×10^6 promastigotes in 2.6 mL) were added to the wells as previously described (Atayde et al., 2019). Parasites were grown in drug-free M199 at 25°C for 7 days. For direct transfer assays, particle preparations (a single dose of 10 μg/mL pure small EVs) were added to 10^6 promastigotes/mL recipient parasite cultures in drug-free M199 at 25°C for 7 days in 24-well plates (Corning, USA). For EV-nucleofection experiments, a total of 15 μg of purified small EVs were directly transfected by nucleofection using the Amaxa Nucleofector System (Lonza) customized for the Human T cell Nucleofector Kit (U-033 program). Selection was achieved in the presence of the drug to which the donor parasites were resistant (25 μM Sb; 1 μM MTX or 120 μg/mL blasticidin S). For all three experimental approaches, recipient parasites were recovered and submitted to different post-exposure tests (drug susceptibility, genomic DNA extraction or microscopy; Tables S3–S5). Experiments were performed with at least three biological replicates from independent cultures, each of which included three technical replicates.

Measurement of reactive oxygen species (ROS) accumulation

Intracellular ROS accumulation was measured using the DCFDA dye (Invitrogen, USA). Briefly, 5×10^7 mid-log *L. infantum* WT promastigotes were exposed to 5 μg/mL purified EVs for 3 h and then exposed to the EC_{90} of the antileishmanial drugs (e.g., Sb, MF or AmB) for 48h in M199 medium at 25°C supplemented with 10% fetal bovine serum and 5 μg/mL of haemin at pH 7.0. Parasites were washed twice in Hepes–NaCl (21 mM HEPES, 137 mM NaCl, 5 mM KCl, 0.7 mM $Na_2HPO_4 \cdot 7H_2O$, 6 mM glucose, pH 7.4) and resuspended in 500 μL of Hepes–NaCl containing 25 μg/mL of H_2DCFDA (Invitrogen, USA). Parasites were then incubated in the dark for 30 min and washed twice with Hepes–NaCl. After washing, 200 μL of the promastigote resuspension was analyzed with a Cytation 5 machine (BioTek, USA) at 485 nm excitation and 535 nm emission wavelengths. Fluorescence was normalized with the number of living parasites determined by PI staining and manual counting. Experiments were performed with at least three biological replicates from independent cultures, each of which included three technical replicates.

LC–MS/MS

Liquid chromatography–MS/MS was performed at the *Institut de Recherches Cliniques de Montréal* (IRCM, Université de Montréal, Canada). Twenty μg of proteins derived from late-logarithmic *L. infantum* promastigotes were precipitated with 15% trichloroacetic acid/acetone and processed as previously described (Atayde et al., 2019; Douanne et al., 2020a). Briefly, proteins were solubilized using a 6M urea buffer, reduced by the addition of reduction buffer (45 mM DTT, 100 mM ammonium bicarbonate) for 30 min at 37°C, and then by the addition of alkylation buffer (100 mM iodoacetamide, 100 mM ammonium bicarbonate) for 20 min at 24°C in the dark. Subsequently, an in-solution digestion was performed by the addition of trypsin at a ratio of 1:25 protease/protein. After an overnight incubation at 37°C, reactions were quenched by adding formic acid to a 0.2% final concentration. Samples were cleaned with C18 Zip Tip pipette tips (Millipore, USA), eluates were dried down in a vacuum centrifuge and then re-solubilized under agitation for 15 min in 10 mL of 2% ACN/1% formic acid. The column was installed on the Easy-LLC II system (Proxeon Biosystems, Odense, Denmark) and coupled to the LTQ Orbitrap Velos (ThermoFisher Scientific, Bremen, Germany) equipped with a Proxeon nanoelectrospray ion source. Proteomic experiments were performed with at least three biological replicates from independent cultures.

Database searching and protein identification

All MS/MS samples were analyzed using Mascot (Matrix Science, London, UK; version Mascot in Proteome Discoverer 2.4.0.305). Mascot was set up to search UniProt_*Leishmania_Infantum*_JPCM5, assuming the digestion enzyme trypsin. Mascot was searched with a fragment ion mass tolerance of 0.050 Da and a parent ion tolerance of 10.0 PPM. Carbamidomethyl of cysteine was specified in Mascot as a fixed modification, and oxidation of methionine as a variable modification. Next, validation of MS/MS-based peptide and protein identifications were performed using Scaffold (Scaffold_4.9.0 version, Proteome Software Inc., Portland, USA). Peptide identifications were accepted if they could be established at greater than 80.0% probability by the Peptide Prophet algorithm. Protein identifications were accepted if they could be established at greater than 99.0% probability and contained at least 2 identified peptides. Protein probabilities were assigned by the Protein Prophet algorithm. Proteins that contained similar peptides and could not be differentiated based on MS/MS analysis alone were grouped to satisfy the principles of parsimony. Finally, proteins sharing significant peptide evidence were grouped into clusters.

Proteomics analysis

The results of the LC-MS/MS were imported and normalized with the Scaffold (version 4.11.0) software. Only proteins with at least 2 normalized spectrum counts in a minimum of three samples were retained for downstream analyses. Protein information was completed with UniprotKB (UniProt, 2019) and TriTrypDB v46 (Aslett et al., 2010) databases. To identify differentially expressed proteins, an adjusted T test p value < 0.05 and fold-change (FC) ≥ 2 for upregulated proteins and FC ≤ 0.5 for downregulated proteins

were set as thresholds to define the significance. Blast2GO version 6.0.1 was used to map the differentially expressed proteins in the gene ontology (GO) database (Gotz et al., 2008).

QUANTIFICATION AND STATISTICAL ANALYSIS

To evaluate the differences between the samples studied, statistical analyses were performed using multiple one-sided unpaired t test (*$p \leq 0.05$, **$p \leq 0.01$, ***$p \leq 0.001$, ****$p \leq 0.0001$). In the different experiments, each data point represents the average ± SEM (n = 3). The data were analyzed using GraphPad Prism 8.0 software (GraphPad Software, La Jolla California, USA). The results are representative of at least three independent experiments.